Consolidated Project Report

Reimann Problem for Hyperbolic System of Partial Differential Equations

VIDIT GOYAL-2021B4AA2944G

KALASH PODDAR – 2021B4AA3025G

LAKSHAY SHEWANI – 2021B4AA2786G

Prepared in partial fulfilment of the Study Oriented Project

Course No: MATH F266

AT

KK BIRLA, BITS PILANI,
GOA CAMPUS

ABSTRACT

The "Riemann Problem for Hyperbolic Systems of Partial Differential Equations" poses a significant challenge in computational mathematics and fluid dynamics. This project focuses on investigating and comparing four prominent numerical schemes—Lax-Friedrichs, Lax-Wendroff, Warming-Beam, and Godunov—for solving this complex problem. Each scheme offers distinct advantages and limitations in approximating solutions to hyperbolic systems, motivating a comparative analysis to discern their efficacy across various scenarios. Employing rigorous mathematical formulations and computational simulations, this study delves into the behavior of these schemes under diverse conditions, aiming to elucidate their respective strengths and weaknesses. Through meticulous examination of numerical accuracy, stability, and computational efficiency, this research contributes to a deeper understanding of numerical methods for hyperbolic systems. By synthesizing theoretical insights with computational results, this investigation provides valuable insights into the practical applicability of these schemes, paving the way for informed decision-making in computational fluid dynamics and related fields.

INDEX

1: Notions on Hyperbolic Partial Differential Equations

1.1 Quasi-Linear Equations: Basic Concepts

In this section we study systems of first-order partial differential equations of the form

$$\frac{\partial u_i}{\partial t} + \sum_{j=1}^{m} a_{ij}(x, t, u_1, \dots, u_m) \frac{\partial u_j}{\partial x} + b_i(x, t, u_1, \dots, u_m) = 0 \tag{1.1}$$

for $i = 1, \dots, m$. This is a system of m equations in m unknowns u_i that depend on space x and a time-like variable t. Here u_i are the dependent variables and x, t are the independent variables; this is expressed via the notation $u_i = u_i(x, t)$; $\partial u_i / \partial t$ denotes the partial derivative of $u_i(x, t)$ with respect to t; similarly $\partial u_i / \partial x$ denotes the partial derivative of $u_i(x, t)$ with respect to x. We also make use of subscripts to denote partial derivatives. System (1.1) can also be written in matrix form as

$$\mathbf{U}_t + \mathbf{A}\mathbf{U}_x + \mathbf{B} = \mathbf{0} \tag{1.2}$$

with

$$\mathbf{U} = \begin{bmatrix} u_1 \\ u_2 \\ \vdots \\ u_m \end{bmatrix}, \mathbf{B} = \begin{bmatrix} b_1 \\ b_2 \\ \vdots \\ b_m \end{bmatrix}, \mathbf{A} = \begin{bmatrix} a_{11} & \dots & a_{1m} \\ a_{21} & \dots & a_{2m} \\ \vdots & \vdots & \vdots \\ a_{m1} & \dots & a_{mm} \end{bmatrix} \tag{1.3}$$

If the entries a_{ij} of the matrix **A** are all constant and the components b_j of the vector **B** are also constant then system (1.2) is linear with constant coefficients. If $a_{ij} = a_{ij}(x, t)$ and $b_i = b_i(x, t)$ the system is linear with variable coefficients. The system is still linear if **B** depends linearly on **U** and is called quasi-linear if the coefficient matrix **A** is a function of the vector **U**, that is $\mathbf{A} = \mathbf{A}(\mathbf{U})$. Note that quasi-linear systems are in general systems of non-linear equations. System (1.2) is called homogeneous if $\mathbf{B} = \mathbf{0}$. For a set of PDEs of the form (1.2) one needs to specify the range of variation of the independent variables x and t. Usually x lies in a subinterval of the real line, namely $x_1 < x < x_\mathrm{r}$; this subinterval is called the spatial domain of the PDEs, or just domain. At the values x_1, x_r one also needs to specify Boundary Conditions (BCs). In this Chapter we assume the domain is the full real line, $-\infty < x < \infty$, and thus no boundary conditions need to be specified. As to variations of time t we assume $t_0 < t < \infty$. An Initial Condition (IC) needs to be specified at the initial time, which is usually chosen to be $t_0 = 0$.

Two scalar ($m = 1$) examples of PDEs of the form (1.1) are the linear advection equation

$$\frac{\partial u}{\partial t} + a\frac{\partial u}{\partial x} = 0 \tag{1.4}$$

and the inviscid Burgers equation

$$\frac{\partial u}{\partial t} + u\frac{\partial u}{\partial x} = 0 \tag{1.5}$$

In the linear advection equation (1.4) the coefficient a (a constant) is the wave propagation speed. In the Burgers equation $a = a(u) = u$.

Definition 1.1 (Conservation Laws): Conservation laws are systems of partial differential equations that can be written in the form

$$\mathbf{U}_t + \mathbf{F}(\mathbf{U})_x = \mathbf{0} \tag{1.6}$$

where

$$\mathbf{U} = \begin{bmatrix} u_1 \\ u_2 \\ \vdots \\ u_m \end{bmatrix}, \ \mathbf{F}(\mathbf{U}) = \begin{bmatrix} f_1 \\ f_2 \\ \vdots \\ f_m \end{bmatrix} \tag{1.7}$$

$\mathbf{U}$ is called the vector of conserved variables, $\mathbf{F} = \mathbf{F}(\mathbf{U})$ is the vector of fluxes and each of its components f_i is a function of the components u_j of $\mathbf{U}$.

Definition 1.2 (Jacobian Matrix): The Jacobian of the flux function $\mathbf{F}(\mathbf{U})$ in (1.6) is the matrix

$$\mathbf{A}(\mathbf{U}) = \partial\mathbf{F}/\,\partial\mathbf{U} = \begin{bmatrix} \partial f_1/\,\partial u_1 & \dots & \partial f_1/\,\partial u_m \\ \partial f_2/\,\partial u_1 & \dots & \partial f_2/\,\partial u_m \\ \vdots & \vdots & \vdots \\ \partial f_m/\,\partial u_1 & \dots & \partial f_m/\,\partial u_m \end{bmatrix} \tag{1.8}$$

The entries a_{ij} of $\mathbf{A}(\mathbf{U})$ are partial derivatives of the components f_i of the vector $\mathbf{F}$ with respect to the components u_j of the vector of conserved variables $\mathbf{U}$, that is $a_{ij} = \partial f_i/\,\partial u_j$.

Note that conservation laws of the form (1.6)-(1.7) can also be written in quasi-linear form (1.2), with $\mathbf{B} \equiv \mathbf{0}$, by applying the chain rule to the second term in (1.6), namely

$$\frac{\partial \mathbf{F}(\mathbf{U})}{\partial x} = \frac{\partial \mathbf{F}}{\partial \mathbf{U}}\frac{\partial \mathbf{U}}{\partial x}$$

Hence (1.6) becomes

$$\mathbf{U}_t + \mathbf{A}(\mathbf{U})\mathbf{U}_x = \mathbf{0}$$

which is a special case of (1.2). The scalar PDEs (1.4) and (1.5) can be expressed as conservation laws, namely

$$\frac{\partial u}{\partial t}+\frac{\partial f(u)}{\partial x}=0, f(u)=au \tag{1.9}$$

$$\frac{\partial u}{\partial t}+\frac{\partial f(u)}{\partial x}=0, f(u)=\frac{1}{2}u^2 \tag{1.10}$$

Definition 1.3 (Eigenvalues): The eigenvalues λ_i of a matrix **A** are the solutions of the characteristic polynomial

$$|\mathbf{A}-\lambda\mathbf{I}|=\det(\mathbf{A}-\lambda\mathbf{I})=0 \tag{1.11}$$

where **I** is the identity matrix. The eigenvalues of the coefficient matrix **A** of a system of the form (1.2) are called the eigenvalues of the system.

Physically, eigenvalues represent speeds of propagation of information. Speeds will be measured positive in the direction of increasing x and negative otherwise.

Definition 1.4 (Eigenvectors): A right eigenvector of a matrix A corresponding to an eigenvalue λ_i of **A** is a vector $\mathbf{K}^{(i)}=\left[k_1^{(i)},k_2^{(i)},\dots,k_m^{(i)}\right]^T$ satisfying $\mathbf{A}\mathbf{K}^{(i)}=\lambda_i\mathbf{K}^{(i)}$. Similarly, a left eigenvector of a matrix **A** corresponding to an eigenvalue λ_i of **A** is a vector $\mathbf{L}^{(i)}=\left[l_1^{(i)},l_2^{(i)},\dots,l_m^{(i)}\right]$ such that $\mathbf{L}^{(i)}\mathbf{A}=\lambda_i\mathbf{L}^{(i)}$.

For the scalar examples (1.9) − (1.10) the eigenvalues are trivially found to be $\lambda=a$ and $\lambda=u$ respectively. Next we find eigenvalues and eigenvectors for a system of PDEs.

Example 2.1 (Linearized Gas Dynamics): The linearized equations of Gas Dynamics are the 2×2 linear system

$$\left.\begin{aligned}\frac{\partial\rho}{\partial t}+\rho_0\frac{\partial u}{\partial x}=0,\\ \frac{\partial u}{\partial t}+\frac{a^2}{\rho_0}\frac{\partial\rho}{\partial x}=0\end{aligned}\right\} \tag{1.12}$$

where the unknowns are the density $u_1=\rho(x,t)$ and the speed $u_2=u(x,t)$; ρ_0 is a constant reference density and a is the sound speed, a positive constant. When written in the matrix form (1.2) this system reads

$$\mathbf{U}_t+\mathbf{A}\mathbf{U}_x=\mathbf{0} \tag{1.13}$$

with

$$\mathbf{U}=\begin{bmatrix}u_1\\u_2\end{bmatrix}\equiv\begin{bmatrix}\rho\\u\end{bmatrix},\ \mathbf{A}=\begin{bmatrix}0 & \rho_0\\ a^2/\rho_0 & 0\end{bmatrix} \tag{1.14}$$

The eigenvalues of the system are the zeros of the characteristic polynomial

$$|\mathbf{A}-\lambda\mathbf{I}|=\det\begin{bmatrix}-\lambda-\lambda & \rho_0\\ a^2/\rho_0 & 0-\lambda\end{bmatrix}=0$$

That is, $\lambda^2 = a^2$, which has two real and distinct solutions, namely

$$\lambda_1 = -a,\ \lambda_2 = +a \tag{1.15}$$

We now find the right eigenvectors $\mathbf{K}^{(1)}, \mathbf{K}^{(2)}$ corresponding to the eigenvalues λ_1 and λ_2.

The eigenvector $\mathbf{K}^{(1)}$ for eigenvalue $\lambda = \lambda_1 = -a$ is found as follows: we look for a vector $\mathbf{K}^{(1)} = [k_1, k_2]^T$ such that $\mathbf{K}^{(1)}$ is a right eigenvector of $\mathbf{A}$, that is $\mathbf{A}\mathbf{K}^{(1)} = \lambda_1 \mathbf{K}^{(1)}$. Writing this in full gives

$$\begin{bmatrix} 0 & \rho_0 \\ a^2/\rho_0 & 0 \end{bmatrix} \begin{bmatrix} k_1 \\ k_2 \end{bmatrix} = \begin{bmatrix} -ak_1 \\ -ak_2 \end{bmatrix}$$

which produces two linear algebraic equations for the unknowns k_1 and k_2

$$\rho_0 k_2 = -ak_1,\ \frac{a^2}{\rho_0} k_1 = -ak_2 \tag{1.16}$$

The reader will realise that in fact these two equations are equivalent and so effectively we have a single linear algebraic equation in two unknowns. This gives a one-parameter family of solutions. Thus we select an arbitrary nonzero parameter α_1, a scaling factor, and set $k_1 = \alpha_1$ in any of the equations to obtain $k_2 = -\alpha_1 a/\rho_0$ for the second component and hence the first right eigenvector becomes

$$\mathbf{K}^{(1)} = \alpha_1 \begin{bmatrix} 1 \\ -a/\rho_0 \end{bmatrix} \tag{1.17}$$

The eigenvector $\mathbf{K}^{(2)}$ for eigenvalue $\lambda = \lambda_2 = +a$ is found in a similar manner. The resulting algebraic equations for $\mathbf{K}^{(2)}$ corresponding to the eigenvalue $\lambda_2 = +a$ are

$$\rho_0 k_2 = ak_1,\ \frac{a^2}{\rho_0} k_1 = ak_2 \tag{1.18}$$

By denoting the second scaling factor by α_2 and setting $k_1 = \alpha_2$ we obtain

$$\mathbf{K}^{(2)} = \alpha_2 \begin{bmatrix} 1 \\ a/\rho_0 \end{bmatrix} \tag{1.19}$$

Taking the scaling factors to be $\alpha_1 = \rho_0$ and $\alpha_2 = \rho_0$ gives the right eigenvectors

$$\mathbf{K}^{(1)} = \begin{bmatrix} \rho_0 \\ -a \end{bmatrix},\ \mathbf{K}^{(2)} = \begin{bmatrix} \rho_0 \\ a \end{bmatrix} \tag{1.20}$$

Definition 1.6 (Hyperbolic System): A system (1.2) is said to be hyperbolic at a point (x, t) if $\mathbf{A}$ has m real eigenvalues $\lambda_1, \ldots, \lambda_m$ and a corresponding set of m linearly independent right eigenvectors $\mathbf{K}^{(1)}, \ldots, \mathbf{K}^{(m)}$. The system is said to be strictly hyperbolic if the eigenvalues λ_i are all distinct.

Note that strict hyperbolicity implies hyperbolicity, because real and distinct eigenvalues ensure the existence of a set of linearly independent eigenvectors. The system (1.2) is said to be elliptic at a point (x, t) if none of the eigenvalues λ_i of $\mathbf{A}$ are real. Both scalar

examples (1.9)-(1.10) are trivially hyperbolic. The linearised gas dynamic equations (1.12) are also hyperbolic, since λ_1 and λ_2 are both real at any point (x, t). Moreover, as the eigenvalues are also distinct this system is strictly hyperbolic.

1.2 The Linear Advection Equation

A general, time-dependent linear advection equation in three space dimensions reads

$$u_t + a(x, y, z, t)u_x + b(x, y, z, t)u_y + c(x, y, z, t)u_z = 0 \tag{1.21}$$

where the unknown is $u = u(x, y, z, t)$ and a, b, c are variable coefficients. If the coefficients are sufficiently smooth one can express (1.21) as a conservation law with source terms, namely

$$u_t + (au)_x + (bu)_y + (cu)_z = u\big(a_x + b_y + c_z\big) \tag{1.22}$$

In this section we study in detail the initial-value problem (IVP) for the special case of the linear advection equation, namely

$$\left.\begin{array}{rc} \text{PDE:} & u_t + au_x = 0, -\infty < x < \infty, t > 0 \\ \text{IC:} & u(x, 0) = u_0(x), \end{array}\right\} \tag{1.23}$$

where a is a constant wave propagation speed. The initial data at time $t = 0$ is a function of x alone and is denoted by $u_0(x)$. We warn the reader that for systems we shall use a different notation for the initial data. Generally, we shall not be explicit about the conditions $-\infty < x < \infty; t > 0$ on the independent variables when stating an initial-value problem. The PDE in (1.23) is the simplest hyperbolic PDE and in view of (1.9) is also the simplest hyperbolic conservation law. It is a very useful model equation for the purpose of studying numerical methods for hyperbolic conservation laws, in the same way as the linear, first-order ordinary differential equation

$$\frac{\mathrm{d}x}{\mathrm{d}t} = \beta, x = x(t), \beta = \text{ constant} \tag{1.24}$$

is a popular model equation for analyzing numerical methods for Ordinary Differential Equation (ODEs).

1.2.1 The Riemann Problem

By using geometric arguments we have constructed the analytical solution of the general IVP (1.23) for the linear advection equation. Now we study a special IVP called the Riemann problem

$$\left.\begin{array}{ll} \text{PDE:} & u_t + a u_x = 0 \\ \text{IC:} & u(x,0) = u_0(x) = \begin{cases} u_{\mathrm{L}} \text{ if } x < 0, \\ u_{\mathrm{R}} \text{ if } x > 0, \end{cases} \end{array}\right\} \tag{1.25}$$

where u_{L} (left) and u_{R} (right) are two constant values, as shown in Fig. 1.1. Note that the initial data has a discontinuity at $x = 0$. IVP (1.25) is the simplest initial-value problem one can pose. The trivial case would result when $u_{\mathrm{L}} = u_{\mathrm{R}}$. From the previous discussion on the solution of the general IVP (1.23) we expect any point on the initial profile to propagate a distance $d = at$ in time t. In particular, we expect the initial discontinuity at $x = 0$ to propagate a distance $d = at$ in time t. This particular characteristic curve $x = at$ will then separate those characteristic curves to the left, on which the solution takes on the value u_{L}, from those curves to the right, on which the solution takes on the value u_{R}; see Fig. 1.2. So the solution of the Riemann problem (1.25) is simply

$$u(x,t) = u_0(x - at) = \begin{cases} u_{\mathrm{L}} \text{ if } x - at < 0 \\ u_{\mathrm{R}} \text{ if } x - at > 0 \end{cases} \tag{1.26}$$

Solution (1.26) also follows directly from the general solution namely

$u(x,t) = u_0(x - at)$. From (1.25), $u_0(x - at) = u_{\mathrm{L}}$ if $x - at < 0$

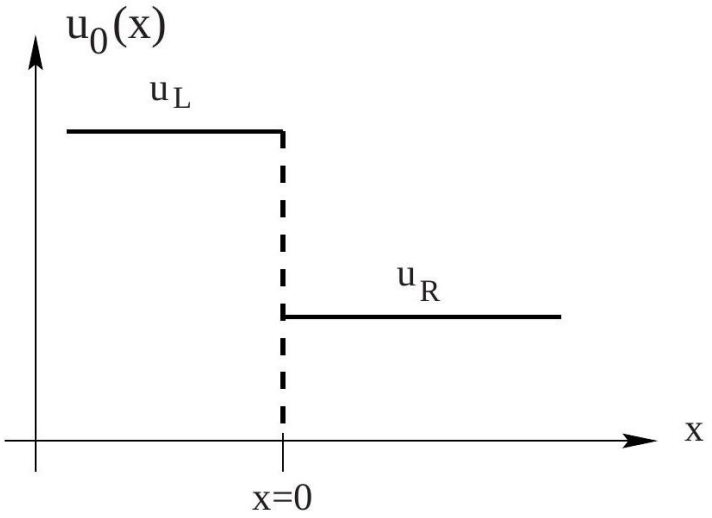

Fig. 1.1. Illustration of the initial data for the Riemann problem. At the initial time the data consists of two constant states separated by a discontinuity at $x = 0$

and $u_0(x - at) = u_R$ if $x - at > 0$. The solution of the Riemann problem can be represented in the $x - t$ plane, as shown in Fig. 1.1. Through any point x_0 on the x-axis one can draw a characteristic. As a is constant these are all parallel to each other. For the solution of the Riemann problem the characteristic that passes through $x = 0$ is significant. This is the only one across which the solution changes.

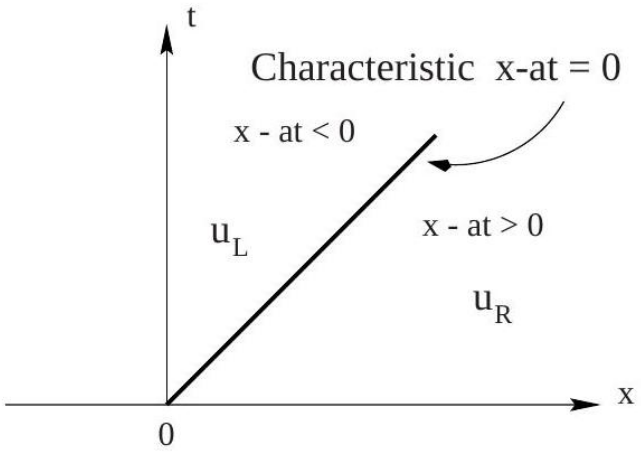

Fig. 1.2. Illustration of the solution of the Riemann problem in the $x - t$ plane for the linear advection equation with positive characteristic speed a

1.3 Linear Hyperbolic Systems

In the previous section we studied in detail the behaviour and the general solution of the simplest PDE of hyperbolic type, namely the linear advection
equation with constant wave propagation speed. Here we extend the analysis to sets of m hyperbolic PDEs of the form

$$\mathbf{U}_t + \mathbf{A}\mathbf{U}_x = \mathbf{0} \tag{1.27}$$

where the coefficient matrix $\mathbf{A}$ is constant. From the assumption of hyperbolicity $\mathbf{A}$ has m real eigenvalues λ_i and m linearly independent eigenvectors $\mathbf{K}^{(i)}, i = 1, \dots, m$.

1.3.1 Diagonalisation and Characteristic Variables

In order to analyse and solve the general IVP for (1.27) it is found useful to transform the dependent variables $\mathbf{U}(x,t)$ to a new set of dependent variables $\mathbf{W}(x,t)$. To this end we recall the following definition

Definition 1.7 (Diagonalisable System): A matrix A is said to be diagonalisable if $\mathbf{A}$ can be expressed as

$$\mathbf{A} = \mathbf{K}\mathbf{\Lambda}\mathbf{K}^{-1} \text{ or } \mathbf{\Lambda} = \mathbf{K}^{-1}\mathbf{A}\mathbf{K}, \tag{1.28}$$

in terms of a diagonal matrix $\mathbf{\Lambda}$ and a matrix $\mathbf{K}$. The diagonal elements of $\mathbf{\Lambda}$ are the eigenvalues λ_i of $\mathbf{A}$ and the columns $\mathbf{K}^{(i)}$ of $\mathbf{K}$ are the right eigenvectors of $\mathbf{A}$ corresponding to the eigenvalues λ_i, that is

$$\mathbf{\Lambda} = \begin{bmatrix} \lambda_1 & \dots & 0 \\ 0 & \dots & 0 \\ \vdots & \vdots & \vdots \\ 0 & \dots & \lambda_m \end{bmatrix}, \mathbf{K} = \left[\mathbf{K}^{(1)}, \dots, \mathbf{K}^{(m)}\right], \mathbf{A}\mathbf{K}^{(i)} = \lambda_i \mathbf{K}^{(i)} \tag{1.29}$$

A system (1.27) is said to be diagonalisable if the coefficient matrix $\mathbf{A}$ is diagonalisable. Based on the concept of diagonalisation one often defines a hyperbolic system (1.27) as a system with real eigenvalues and diagonalisable coefficient matrix.

1.3.2 Some Useful Definitions

Next we recall some standard definitions associated with hyperbolic systems

Definition 1.8 (Domain of Dependence): Recall that for the linear advection equation the solution at a given point $P = (x^*, t^*)$ depends solely on the initial data at a single point x_0 on the x-axis. This point is obtained by tracing back the characteristic passing through the point $P = (x^*, t^*)$. As a matter of fact, the solution at $P = (x^*, t^*)$ is identical to the value of the initial data $u_0(x)$ at the point x_0. One says that the domain of dependence of the point $P = (x^*, t^*)$ is the point x_0. For a 2×2 system the domain of dependence is an interval $[x_L, x_R]$ on the x-axis that is subtended by the characteristics passing through the point $P = (x^*, t^*)$.

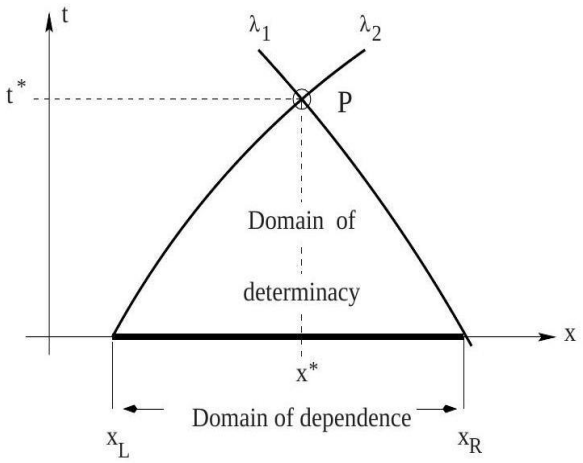

Fig. 1.3. Domain of dependence of point P and corresponding domain of determinacy, for a 2 by 2 system

Fig. 1.3 illustrates the domain of dependence for a 2×2 system with characteristic speeds λ_1 and λ_2, with $\lambda_1 < \lambda_2$. In general, the characteristics of a hyperbolic system are curved. For a larger system the domain of dependence is determined by the slowest and fastest characteristics and is always a bounded interval, as the characteristic speeds for hyperbolic systems are always finite.

Definition 1.9 (Domain of Determinacy). For a given domain of dependence $[x_L, x_R]$, the domain of determinacy is the set of points (x, t), within the domain of existence of the solution $\mathbf{U}(x, t)$, in which $\mathbf{U}(x, t)$ is solely determined by initial data on $[x_L, x_R]$.

In Fig. 1.3 we illustrate the domain of determinacy of an interval $[x_L, x_R]$ for the case of a 2×2 system with characteristic speeds λ_1 and λ_2, with $\lambda_1 < \lambda_2$.

Definition 1.17 (Range of Influence). Another useful concept is that of the range of influence of a point $Q = (x_0, 0)$ on the x-axis. It is defined as the set of points (x, t) in the

$x-t$ plane in which the solution $\mathbf{U}(x,t)$ is influenced by initial data at the point $Q = (x_0, 0)$.

Fig. 1.4 illustrates the range of influence of a point $Q = (x_0, 0)$ for the case of a 2×2 system with characteristic speeds λ_1 and λ_2, with $\lambda_1 < \lambda_2$.

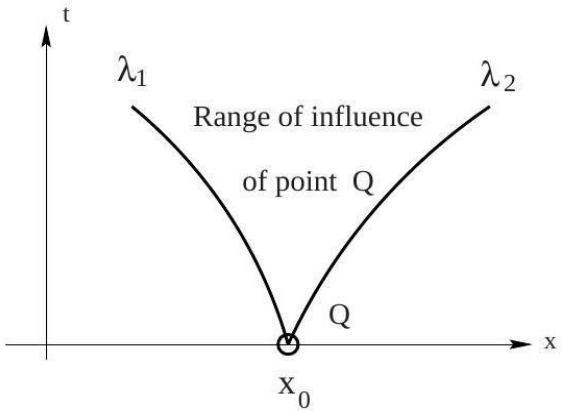

Fig. 1.4. Range of influence of point Q for a 2 by 2 system

has real eigenvalues $\lambda_i(\mathbf{U})$ and a complete set of linearly independent eigenvectors $\mathbf{K}^{(i)}(\mathbf{U}), i = 1, \dots, m$, which we assume to be ordered as

$$\lambda_1(\mathbf{U}) < \lambda_2(\mathbf{U}) <, \dots, < \lambda_m(\mathbf{U})$$
$$\mathbf{K}^{(1)}(\mathbf{U}), \mathbf{K}^{(2)}(\mathbf{U}), \dots, \mathbf{K}^{(m)}(\mathbf{U})$$

Shock Waves

Shock waves in air are small transition layers of very rapid changes of physical quantities such as pressure, density and temperature. The transition layer for a strong shock is of the same order of magnitude as the mean-free path of the molecules, that is about 10^{-7} m. Therefore replacing these waves as mathematical discontinuities is a reasonable approximation. Very weak shock waves such as sonic booms, are an exception; the discontinuous approximation here can be very inaccurate indeed.

We therefore insist on using the simplified model but in its integral formConsider a solution $u(x,t)$ such that $u(x,t), f(u)$ and their derivatives are continuous everywhere except on a line $s = s(t)$ on the $x-t$ plane across which $u(x,t)$ has a jump discontinuity. Select two fixed points x_L and x_R on the x-axis such that $x_\mathrm{L} < s(t) < x_\mathrm{R}$. Enforcing the conservation law in integral form on the control volume $[x_\mathrm{L}, x_\mathrm{R}]$ leads to

$$f\big(u(x_\mathrm{L},t)\big) - f\big(u(x_\mathrm{R},t)\big) = \frac{\mathrm{d}}{\mathrm{d}t}\int_{x_\mathrm{L}}^{s(t)} u(x,t)\mathrm{d}x + \frac{\mathrm{d}}{\mathrm{d}t}\int_{s(t)}^{x_\mathrm{R}} u(x,t)\mathrm{d}x$$

$$f\big(u(x_{\mathrm{L}},t)\big)-f\big(u(x_{\mathrm{R}},t)\big)=\begin{matrix}[u(s_{\mathrm{L}},t)-u(s_{\mathrm{R}},t)]S\\ +\int_{x_{\mathrm{L}}}^{s(t)}u_t(x,t)\mathrm{d}x+\int_{s(t)}^{x_{\mathrm{R}}}u_t(x,t)\mathrm{d}x,\end{matrix}\Bigg\}$$

where $u(s_{\mathrm{L}},t)$ is the limit of $u(s(t),t)$ as x tends to $s(t)$ from the left, $u(s_{\mathrm{R}},t)$ is the limit of $u(s(t),t)$ as x tends to $s(t)$ from the right and $S=\mathrm{d}s/\mathrm{d}t$ is the speed of the discontinuity. As $u_t(x,t)$ is bounded the integrals vanish identically as $s(t)$ is approached from left and right and we obtain

$$f\big(u(x_{\mathrm{L}},t)\big)-f\big(u(x_{\mathrm{R}},t)\big)=[u(s_{\mathrm{L}},t)-u(s_{\mathrm{R}},t)]S \tag{1.30}$$

This algebraic expression relating the jumps $\Delta f=f\big(u(x_{\mathrm{R}},t)\big)-f\big(u(x_{\mathrm{L}},t)\big)$, $\Delta u=u(x_{\mathrm{R}},t)-u(x_{\mathrm{L}},t)$ and the speed S of the discontinuity is called the Rankine-Hugoniot condition and is usually expressed as

$$\Delta f=S\Delta u \tag{1.31}$$

For the scalar case considered here one can solve for the speed S as

$$S=\frac{\Delta f}{\Delta u} \tag{1.32}$$

Therefore, in order to admit discontinuous solutions we may formulate the problem in terms of PDEs, which are valid in smooth parts of the solution, and the Rankine-Hugoniot conditions across discontinuities.

Fig. 1.4. However, this solution is physically incorrect. The discontinuity has not arisen as the result of compression, $\lambda_{\mathrm{L}}<\lambda_{\mathrm{R}}$; the characteristics diverge from the discontinuity. This solution is called a rarefaction shock, or entropy-violating shock, and does not satisfy the entropy condition it is therefore rejected as a physical solution.

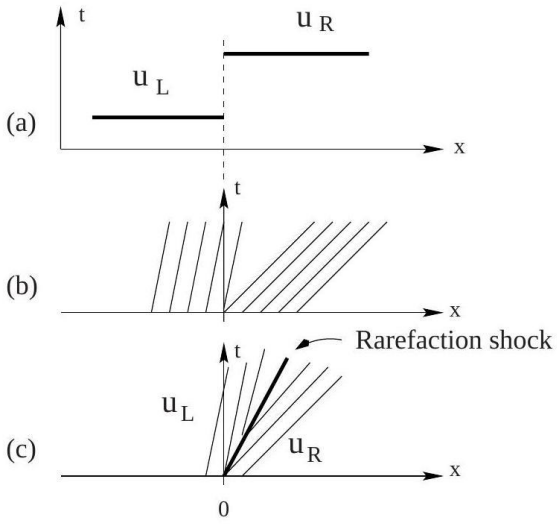

Fig. 1.4. (a) Expansive discontinuous initial data (b) picture of characteristics and (c) rarefaction shock solution on x - t plane

Rarefaction Waves

Reconsider the IVP (2.100) with general convex flux function $f(u)$

$$u_t + f(u)_x = 0 \tag{1.33}$$

$$u(x,0) = u_0(x) = \begin{cases} u_{\mathrm{L}} \text{ if } x < 0 \\ u_{\mathrm{R}} \text{ if } x > 0 \end{cases} \tag{1.33}$$

and expansive initial data, $u_{\mathrm{L}} < u_{\mathrm{R}}$. As discussed previously, the entropyviolating solution to this problem is

$$\left.\begin{aligned} u(x,t) &= \begin{cases} u_{\mathrm{L}} \text{ if } x - St < 0 \\ u_{\mathrm{R}} \text{ if } x - St > 0 \end{cases} \\ S &= \frac{\Delta f}{\Delta u} \end{aligned}\right\} \tag{1.34}$$

Amongst the various other reasons for rejecting this solution as a physical solution, instability stands out as a prominent argument. By instability it is meant that small perturbations of the initial data lead to large changes in the solution. As a matter of fact, under small perturbations, the whole character of the solution changes completely, as we shall see.

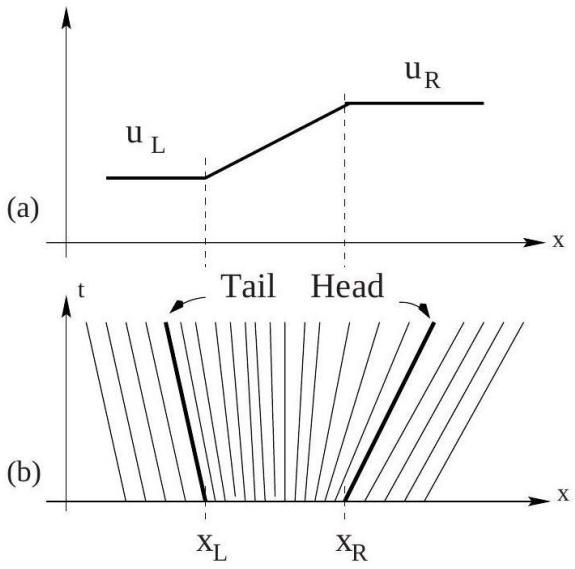

Fig. 1.5. Non-centred rarefaction wave: (a) expansive smooth initial data, (b) picture of characteristics on $x - t$ plane

Let us modify the initial data in (1.33) by replacing the discontinuous change from u_{L} to u_{R} by a linear variation of $u_0(x)$ between two fixed points $x_{\mathrm{L}} < 0$ and $x_{\mathrm{R}} > 0$. Now the initial data reads

$$u_0(x) = \begin{cases} u_{\mathrm{L}} & \text{if} \quad x \le x_{\mathrm{L}} \,, \\ u_{\mathrm{L}} + \frac{u_{\mathrm{R}} - u_{\mathrm{L}}}{x_{\mathrm{R}} - x_{\mathrm{L}}}(x - x_{\mathrm{L}}) & \text{if} \quad x_{\mathrm{L}} < x < x_{\mathrm{R}} \,, \\ u_{\mathrm{R}} & \text{if} \quad x \ge x_{\mathrm{R}} \,, \end{cases}$$

and is illustrated in Fig. 1.5a. The corresponding picture of characteristics emanating from the initial time $t = 0$ is shown in Fig. 1.5b. The solution $u(x,t)$ to this problem is found by following characteristics, as discussed previously, and consists of two constant states, u_{L} and u_{R}, separated by a region of smooth transition between the data values u_{L} and u_{R}. This is called a rarefaction wave. The right edge of the wave is given by the characteristic emanating

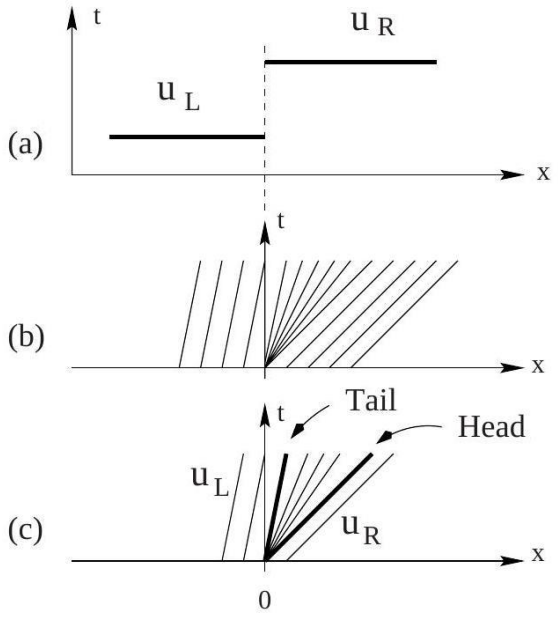

Fig. 1.6. Centred rarefaction wave: (a) expansive discontinuous initial data (b) picture of characteristics (c) entropy satisfying (rarefaction) solution on $x - t$ plane

from x_{R}

$$x = x_{\mathrm{R}} + \lambda(u_{\mathrm{R}})t \tag{1.35}$$

and is called the Head of the rarefaction. It carries the value $u_0(x_{\mathrm{R}}) = u_{\mathrm{R}}$. The left edge of the wave is given by the characteristic emanating from x_{L}

$$x = x_{\mathrm{L}} + \lambda(u_{\mathrm{L}})t \tag{1.36}$$

and is called the Tail of the rarefaction. It carries the value $u_0(x_{\mathrm{L}}) = u_{\mathrm{L}}$.

As we assume convexity, $\lambda'(u) = f''(u) > 0$, larger values of $u_0(x)$ propagate faster than lower values and thus the wave spreads and flattens as time evolves. The spreading of

waves is a typical non-linear phenomenon not seen in the study of linear hyperbolic systems with constant coefficients. The entire solution is

$$\left.\begin{array}{rcll} u(x,t) = & u_{\mathrm{L}} & \text{if} & \frac{x-x_{\mathrm{L}}}{t} \leq \lambda_{\mathrm{L}} \ , \\ \lambda(u) & = \frac{x-x_{\mathrm{L}}}{t} & \text{if} & \lambda_{\mathrm{L}} < \frac{x-x_{\mathrm{L}}}{t} < \lambda_{\mathrm{R}} \ , \\ u(x,t) = & u_{\mathrm{R}} & \text{if} & \frac{x-x_{\mathrm{R}}}{t} \geq \lambda_{\mathrm{R}} \ . \end{array}\right\}$$

No matter how small the size $\Delta x = x_{\mathrm{R}} - x_{\mathrm{L}}$ of the interval over which the discontinuous data in IVP (1.33) has been spread over, the structure of the above rarefaction solution remains unaltered and is entirely different from the rarefaction shock solution (1.34), for which small changes to the data lead to large changes in the solution. Thus the rarefaction shock solution is unstable. From the above construction the rarefaction solution is stable and as x_{L} and x_{R} approach zero from below and above respectively, the discontinuous data at $x = 0$ in IVP (1.33) is reproduced. Therefore, the limiting case is to be
interpreted as follows: $u_0(x)$ takes on all the values between u_{L} and u_{R} at $x = 0$ and consequently $\lambda(u_0(x))$ takes on all the values between λ_{L} and λ_{R} at $x = 0$. As higher values propagate faster than lower values the initial data disintegrates immediately giving rise to a rarefaction solution. This limiting rarefaction in which all characteristics of the wave emanate from a single point is called a centred rarefaction wave. The solution is

$$\left.\begin{array}{rcll} u(x,t) = u_{\mathrm{L}} & \text{if} & \frac{x}{t} \leq \lambda_{\mathrm{L}} \ , \\ \lambda(u) \ = \ \frac{x}{t} & \text{if} & \lambda_{\mathrm{L}} < \frac{x}{t} < \lambda_{\mathrm{R}} \ , \\ u(x,t) = u_{\mathrm{R}} & \text{if} & \frac{x}{t} \geq \lambda_{\mathrm{R}} \ , \end{array}\right\}$$

and is illustrated in Fig. 1.6.

Now we have at least two solutions to the IVP (1.33). Thus, having extended the concept of solution to include discontinuities, extra spurious solutions are now part of this extended class. The question is how to distinguish between a physically correct solution and a spurious solution. The anticipated answer is that a physical discontinuity, in addition to the Rankine-Hugoniot condition, also satisfies the entropy condition .

The Riemann Problem for the Inviscid Burgers Equation

We finalise this section by giving the solution of the Riemann problem for the inviscid Burgers equation, namely

$$\text{PDE: } u_t + \left(\frac{u^2}{2}\right)_x = 0 \tag{1.37}$$

$$\text{IC: } u(x,0) = \begin{cases} u_{\mathrm{L}}, x < 0 \\ u_{\mathrm{R}}, x > 0 \end{cases} \tag{1.37}$$

From the previous discussion the exact solution is a single wave emanating from the origin as shown in Fig. 1.7a. In view of the entropy condition this wave is either a shock wave, when $u_{\mathrm{L}} > u_{\mathrm{R}}$, or a rarefaction wave, when $u_{\mathrm{L}} \leq u_{\mathrm{R}}$. The complete solution is

$$
\left.
\begin{aligned}
u(x,t) &= \left.\begin{cases} u_{\mathrm{L}} & \text{if } x - St < 0 \\ u_{\mathrm{R}} & \text{if } x - St > 0 \end{cases}\right\} \text{if } u_{\mathrm{L}} > u_{\mathrm{R}} \\
S &= \frac{1}{2}(u_{\mathrm{L}} + u_{\mathrm{R}}) \\
u(x,t) &= \left.\begin{cases} u_{\mathrm{L}} & \text{if } \dfrac{x}{t} \le u_{\mathrm{L}} \\ \dfrac{x}{t} & \text{if } u_{\mathrm{L}} < x/t < u_{\mathrm{R}} \\ u_{\mathrm{R}} & \text{if } x/t \ge u_{\mathrm{R}} \end{cases}\right\} \text{if } u_{\mathrm{L}} \le u_{\mathrm{R}}
\end{aligned}
\right\} \tag{1.38}
$$

Fig. 1.7 shows the solution of the Riemann problem for the inviscid Burgers equation. Fig. 1.7a depicts the structure of the general solution and consists of a single wave, Fig. 1.7b shows the case in which the solution is a shock wave and Fig. 1.7c shows the case in which it is a rarefaction wave.

Some of the studied notions for scalar conservations laws extend quite directly to systems of hyperbolic conservations laws, as we see in the next section.

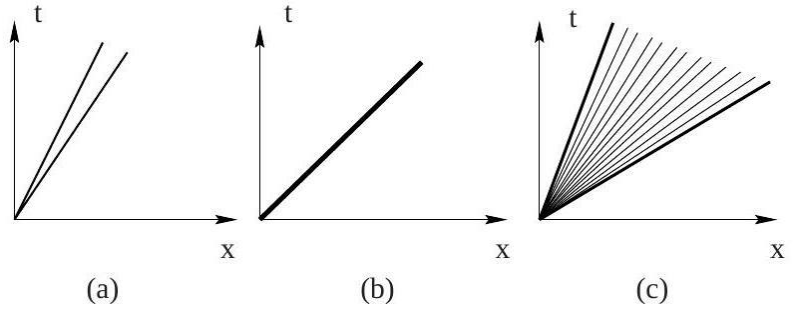

Fig. 1.7. Solution of the Riemann problem for the inviscid Burgers equation: (a) structure of general solution (single wave, shock or rarefaction), (b) solution is a shock wave and (c) solution is a rarefaction wave

2: One Dimensional Euler Equations

Here, we use both conservative and non-conservative formulas to examine the one-dimensional time-dependent Euler equations with an ideal Equation of State. An outline of the fundamental structure of the Riemann issue solution is provided.

2.1 Conservative Formulation

The conservative formulation of the Euler equations, in differential form, is

$$\mathbf{U}_t + \mathbf{F}(\mathbf{U})_x = \mathbf{0}$$

where **U** and **F**(**U**) are the vectors of conserved variables and fluxes, given respectively by,

$$\mathbf{U} = \begin{bmatrix} u_1 \\ u_2 \\ u_3 \end{bmatrix} = \begin{bmatrix} \rho \\ \rho u \\ E \end{bmatrix}$$

$$\mathbf{F}(\mathbf{U}) = \begin{bmatrix} f_1 \\ f_2 \\ f_3 \end{bmatrix} = \begin{bmatrix} \rho u \\ \rho u^2 + p \\ u(E + p) \end{bmatrix}$$

Here p is density, p is pressure, u is particle velocity and E is total energy per unit volume.

$$E = \left(\frac{1}{2}u^2 + e\right)\rho$$

where e is the specific internal energy given by a caloric Equation of State,

$$e = e(\rho, p) = \frac{p}{(\gamma - 1)\rho}$$

Such Conservation laws can be written in Quasi Linear form as,

$$\mathbf{U}_t + \mathbf{A}(\mathbf{U})\mathbf{U}_x = 0$$

where,

$$\mathbf{A}(\mathbf{U}) = \begin{bmatrix} \frac{\partial f_1}{\partial u_1} & \frac{\partial f_1}{\partial u_2} & \frac{\partial f_1}{\partial u_3} \\ \frac{\partial f_2}{\partial u_1} & \frac{\partial f_2}{\partial u_2} & \frac{\partial f_2}{\partial u_3} \\ \frac{\partial f_3}{\partial u_1} & \frac{\partial f_3}{\partial u_2} & \frac{\partial f_3}{\partial u_3} \end{bmatrix}$$

2.2 Non Conservative Formulation

2.2.1 Primitive Variable Formulation

It is possible to formulate and solve the equations using variables other than the conserved variables in order to achieve smooth solutions.

Selecting a vector is one option for the one-dimensional scenario. So we choose

$$\mathbf{W} = (\rho, u, p)^{\mathrm{T}}.$$

The proof is as follows :

We have,

$$\mathbf{U}_{\mathrm{t}} + \mathbf{F}(\mathbf{U})_{\mathrm{x}} = 0$$

where,

$$\mathbf{U} = \begin{bmatrix} u_1 \\ u_2 \\ u_3 \end{bmatrix} = \begin{bmatrix} \rho \\ \rho u \\ E \end{bmatrix}$$

$$\mathbf{F}(\mathbf{U}) = \begin{bmatrix} f_1 \\ f_2 \\ f_3 \end{bmatrix} = \begin{bmatrix} \rho u \\ \rho u^2 + p \\ u(E + p) \end{bmatrix}$$

Now on substitution and partially differentiating, we get

$$\rho_{\mathrm{t}} + u\rho_{\mathrm{x}} + \rho u_{\mathrm{x}} = 0 - - - -(1)$$

and from the 2nd row, we get the second equation as,

$$\rho_{\mathrm{t}} u + u_{\mathrm{t}}\rho + \rho_{\mathrm{x}} u^2 + 2uu_{\mathrm{x}}\rho + \rho_{\mathrm{x}} = 0 - - - (2)$$

On rearranging (2) we get,

$$u[\rho_t + u\rho_x + \rho u_x] + \rho\left[u_t + uu_x + \frac{\rho_x}{\rho}\right] = 0 - - - (3)$$

and on substituting (2) in (3), we get

$$\left[u_t + uu_x + \frac{\rho_x}{\rho}\right] = 0 - - - - (4)$$

Now, from the 3rd row we obtain, and using appropriate substitution, we get

$$\rho_t + \rho u^2 u_x + u p_x = 0 - - - - (5)$$

In Matrix notation, we can write it as,

$$\mathbf{W}_t + \mathbf{A}(\mathbf{W})\mathbf{W}_x = 0$$

where,

$$\mathbf{W} = \begin{bmatrix} \rho \\ u \\ p \end{bmatrix},\ \mathbf{A}(\mathbf{W}) = \begin{bmatrix} u & \rho & 0 \\ 0 & u & \frac{1}{\rho} \\ 0 & \rho a^2 & u \end{bmatrix}$$

One May also find the Eigen values and Eigen Vectors of this system, using $|A - \lambda I| = 0$, getting

$$\begin{vmatrix} u-\lambda & \rho & 0 \\ 0 & u-\lambda & \frac{1}{\rho} \\ 0 & \rho a^2 & u-\lambda \end{vmatrix} = 0 \qquad (1)$$

On solving this the Eigen values and Eigen vectors come out to be,

2.3 Elementary Wave Solutions to Reimann Problem

The Riemann problem for the one-dimensional, time dependent Euler equations with with data $(\mathbf{U_L}, \mathbf{U_R})$ is the IVP

$$\mathbf{U}_t + \mathbf{F}(\mathbf{U})_x = \mathbf{0}$$
$$\mathbf{U}(\mathbf{x}, \mathbf{0}) = \mathbf{U}^0(\mathbf{x}) = \begin{cases} U_L & \text{if } x < 0 \\ U_R & \text{if } x > 0 \end{cases}$$

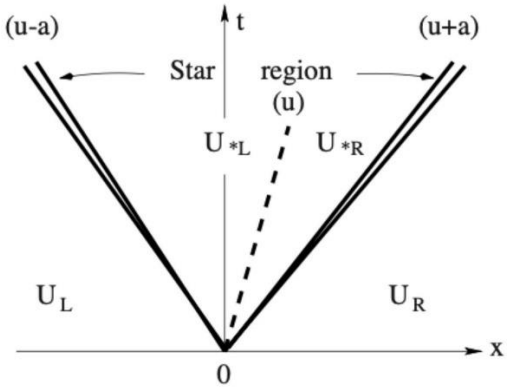

Figure 1: Structure of the solution of the Riemann problem in the x − t plane for the time-dependent, one-dimensional Euler equations. There are three wave families associated with the eigenvalues $u - a, u$ and $u + a$

The three characteristic fields that correspond to the eigenvectors K(i), i = 1,2,3, are connected with three waves. When the character of the
outer waves is uncertain, we follow the norm of depicting them as two rays coming from the origin for the outer waves and a dashed line for the central wave. Each wave family and its related eigenvalue are displayed. Four steady states are divided by the three waves. The wave associated with the $K(2)$ characteristic field is a contact discontinuity and those associated with the $\mathrm{K}(1), \mathrm{K}(3)$ characteristic fields will either be rarefaction waves (smooth) or shock waves (discontinuities). The only exception is the middle wave, which is always a contact discontinuity.

The Figure below shows a particular case in which the left wave is a rarefaction, the middle wave is a contact and the right wave is a shock wave.

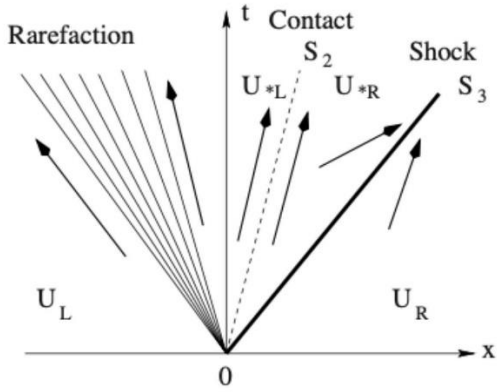

Figure 2: Structure of the solution of the Riemann problem in the x – t plane for the time-dependent, one-dimensional Euler equations, in which the left wave is a rarefaction, the middle wave is a contact discontinuity and the right wave is a shock wave

For the rarefaction wave we have, (S_3 is the speed of shock)

$$\lambda_1(U_{\mathrm{L}}) \leq \lambda_1(U_{\mathrm{R}})$$

For the shock wave we have,

$$\lambda_3(U*_{\mathrm{R}}) > S_3 > \lambda_3(U*_{\mathrm{L}})$$

For the contact wave we have, (S_2 is the speed of the contact wave)

$$\lambda_2(U*_{\mathrm{L}}) = S_2 = \lambda_2(U*_{\mathrm{R}})$$

In the Upcoming sections, we look at each of the wave types separately.

2.3.1 Contact Discontinuities

Suppose, we have a system like,

$$\mathbf{U}_{\mathrm{t}} + \mathbf{F}(\mathbf{U})_{\mathrm{x}} = \mathbf{0}$$

where **U** and **F**(**U**) are the vectors of conserved variables and fluxes, given respectively by,

$$\mathbf{U} = \begin{bmatrix} u_1 \\ u_2 \\ u_3 \end{bmatrix} = \begin{bmatrix} \rho \\ \rho u \\ E \end{bmatrix}$$

$$\mathbf{F}(\mathbf{U}) = \begin{bmatrix} f_1 \\ f_2 \\ f_3 \end{bmatrix} = \begin{bmatrix} \rho u \\ \rho u^2 + p \\ u(E+p) \end{bmatrix}$$

or say in general with,

$$\mathbf{W} = [w_1, w_2, \dots, w_{\mathrm{m}}]^{\mathrm{T}}$$

and the Right Eigen vectors as,

$$K^{(\mathrm{i})} = \left[k_1{}^{(\mathrm{i})}, k_2{}^{(\mathrm{i})}, \ldots, k_\mathrm{m}{}^{(\mathrm{i})}\right]$$

We can write the i[th] Generalised Reimann Invariant as the (m-1) ODEs

$$\frac{dw_1}{k_1^{(\mathrm{i})}} = \frac{dw_2}{k_2^{(\mathrm{i})}} = \cdots = \frac{dw_\mathrm{m}}{k_\mathrm{m}{}^{(\mathrm{i})}}$$

So in applying this on our system, we get

$$\frac{d\rho}{1} = \frac{d(\rho u)}{u} = \frac{E}{\frac{1}{2}u^2}$$

Manipulation gives us,

$$\mathbf{p} = \text{ constant }, \mathbf{u} = \text{ constant}$$

So in short, Contact wave is a discontinuous wave across which both pressure and particle velocity are constant, but density jumps discontinuously as do variables that depend on density, such as specific internal energy, temperature, sound speed, entropy, etc.

2.3.2 Rarefaction Waves

In the Euler equations, the $K^{(1)}$ and $K^{(3)}$ characteristic fields are related to rarefaction waves. Upon examining the eigenvectors for the primitive-variable formulation, it can be observed that ρ, u and p undergo changes throughout a rarefaction wave. Using Entropy Formulation, we have

$$\mathbf{A}(\mathbf{W}) = \begin{bmatrix} u & \rho & 0 \\ \frac{a^2}{\rho} & u & \frac{1}{\rho}\frac{\partial p}{\partial s} \\ 0 & 0 & u \end{bmatrix}$$

On Solving for the Eigen values and Eigen vectors, we get

$$\lambda_1 = u - a, \mathbf{K}^{(1)} = \begin{bmatrix} 1 \\ \frac{-a}{\rho} \\ 0 \end{bmatrix}$$

$$\lambda_2 = u, \mathbf{K}^{(2)} = \begin{bmatrix} -\frac{\partial \rho}{\partial s} \\ 0 \\ a^2 \end{bmatrix}$$

$$\lambda_3 = u + a, \mathbf{K}^{(3)} = \begin{bmatrix} 1 \\ \frac{a}{\rho} \\ 0 \end{bmatrix}$$

For K^1, using the Generalised Reimann Invariants,

$$\frac{d\rho}{1} = \frac{d(u)}{\frac{-a}{\rho}} = \frac{ds}{0}$$

From this we get,

$$s = \text{ Constant}$$
$$du + a\rho d\rho = 0$$

Integrating the 2nd equation, we get

$$u + \int \frac{a}{\rho} d\rho = \text{ constant } - - - (1)$$

Now the Isentropic law states that $p = C\rho^{\gamma}$, i.e $\left(\frac{p}{c}\right)^{\frac{1}{\gamma}} = \rho$, and we also know that $a = \sqrt{\frac{\gamma p}{\rho}}$, using these we get,

$$a = \sqrt{C\gamma}\rho^{\frac{\gamma-1}{2}}$$

Substituting for a in equation (1), we get

$$u + \int \frac{a}{\rho} d\rho => u + \sqrt{C\gamma} \int \rho^{\frac{\gamma-3}{2}} d\rho => 2\sqrt{C\gamma} \frac{\rho^{\frac{\gamma-1}{2}}}{\gamma - 1} => \frac{2a}{\gamma - 1}$$

So finally, we obtain,

$$\mathbf{u} + \frac{2\text{a}}{\gamma - 1} = \text{ constant}$$

Similarly we can get the following condition for $\mathbf{K}^{(3)}$,

$$\mathbf{u} - \frac{2\mathbf{a}}{\gamma - 1} = \text{ constant}$$

To summarise: a rarefaction wave is a smooth wave associated with the 1 and 3 fields across which ρ, u and p change. The wave has a fan-type shape and is enclosed by two bounding characteristics corresponding to the Head and the Tail of the wave.

2.3.3 Shock Waves

Shock waves are discontinuous waves associated with the genuinely non-linear fields 1 and 3. All three quantities ρ, u and p change across a shock wave. Consider the $K^{(3)}$ characteristic field and assume the corresponding wave is a right-facing shock wave travelling at the constant speed S3; see Fig,

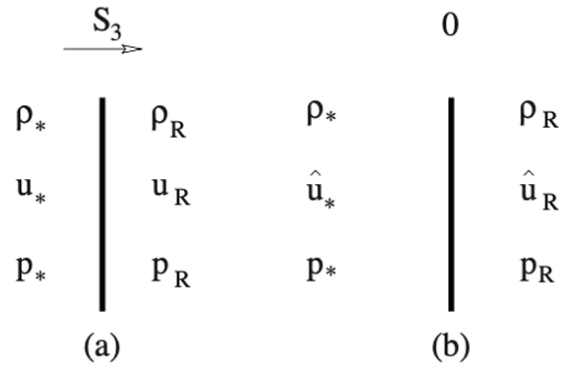

Figure 3: Shock wave facing right: (a) With a stationary frame of reference, the shock has a speed of S3; (b) A moving frame of reference causes the shock to have a speed of zero.

Let the state behind the shock be $\mathbf{W}_* = (\rho_*, u_*, p_*)^{\mathrm{T}}$ and the state ahead of the shock be $\mathbf{W}_{\mathrm{R}} = (\rho_{\mathrm{R}}, u_{\mathrm{R}}, p_{\mathrm{R}})^{\mathrm{T}}$. Densities and pressures remain unaltered while velocities have changed to the relative velocities $\hat{u}_{\mathrm{R}}$ and $\hat{u} *$ given by,

$$\hat{u}_{\mathrm{R}} = u_{\mathrm{R}} - S_3,\ \hat{u} *= u * - S_3$$

Applying the Rankine Hugoniot conditions, we get

$$\rho * \hat{u_*} = \rho_{\mathrm{R}} \hat{u_{\mathrm{R}}}$$
$$\rho_* \hat{u*}^2 + p_* = \rho_{\mathrm{R}} \hat{u_{\mathrm{R}}} + p_{\mathrm{R}}$$
$$u_* \left(\hat{E_*} + p_*\right) = u_{\mathrm{R}} \left(\hat{E_{\mathrm{R}}} + p_{\mathrm{R}}\right)$$

Using the Definitions of Total Energy E, specific internal Energy e , specific enthalpy h and caloric equations of state, followed by algrabic Modifications, we get the following Relations, (For a detailed derivation refer [1])

$$\hat{u_*^2} = \left(\frac{\rho_{\mathrm{R}}}{\rho_*}\right)\left[\frac{p_{\mathrm{R}} - p_*}{\rho_{\mathrm{R}} - \rho_*}\right],\ \hat{u_{\mathrm{R}}} = \left(\frac{\rho^*}{\rho_{\mathrm{R}}}\right)\left[\frac{p_{\mathrm{R}} - p*}{\rho_{\mathrm{R}} - \rho_*}\right]$$
$$h_* - h_{\mathrm{R}} = \left(\frac{1}{2}\right)(p* - p_{\mathrm{R}})\left[\frac{\rho* + \rho_{\mathrm{R}}}{\rho_* \rho_{\mathrm{R}}}\right],\ e_* - e_{\mathrm{R}} = \left(\frac{1}{2}\right)(p_* + p_{\mathrm{R}})\left[\frac{\rho* - \rho_{\mathrm{R}}}{\rho_* \rho_{\mathrm{R}}}\right]$$
$$\frac{\rho *}{\rho_{\mathrm{R}}} = \left[\frac{\left(\frac{p_*}{p_{\mathrm{R}}}\right) + \left(\frac{\gamma - 1}{\gamma + 1}\right)}{\left(\frac{\gamma - 1}{\gamma + 1}\right)\left(\frac{p_*}{p_{\mathrm{R}}}\right) + 1}\right]$$

Now Introducing Mach Numbers, $M_{\mathrm{R}} = \frac{u_{\mathrm{R}}}{a_{\mathrm{R}}}, M_{\mathrm{S}} = \frac{S_3}{a_{\mathrm{R}}}$,

$$\frac{\rho^*}{\rho_{\mathrm{R}}} = \left[\frac{(\gamma+1)(M_{\mathrm{R}} - M_{\mathrm{S}})^2}{(\gamma-1)(M_{\mathrm{R}} - M_{\mathrm{S}})^2 + 1}\right]$$

And the shock speed as a function of pressure ratio across the shock is,

$$S_3 = u_{\mathrm{R}} + a_{\mathrm{R}}\sqrt{\left(\frac{\gamma+1}{2\gamma}\right)\left(\frac{p_*}{p_{\mathrm{R}}}\right) + \left(\frac{\gamma-1}{2\gamma}\right)}$$

The analysis is exactly the same for a 1 -shock wave (left facing) moving at velocity S_1.

3: The Riemann Problem for the Euler Equations

3.1 Equations for Pressure and Particle Velocity

Here we establish equations and solution strategies for computing the pressure p_* and the particle velocity u_* in the Star Region.

Proposition 3.1 (solution for p_* and u_*). The solution for pressure p_* of the Riemann problem with the ideal gas Equation of State is given by the root of the algebraic equation

$$f(p, \mathbf{W}_\mathrm{L}, \mathbf{W}_\mathrm{R}) \equiv f_\mathrm{L}(p, \mathbf{W}_\mathrm{L}) + f_\mathrm{R}(p, \mathbf{W}_\mathrm{R}) + \Delta u = 0, \Delta u \equiv u_\mathrm{R} - u_\mathrm{L} \tag{3.1}$$

where the function f_L is given by

$$f_\mathrm{L}(p, \mathbf{W}_\mathrm{L}) = \begin{cases} (p - p_\mathrm{L}) \left[\frac{A_\mathrm{L}}{p + B_\mathrm{L}} \right]^{\frac{1}{2}} & \text{if } p > p_\mathrm{L} \text{ (shock)} \ , \\ \frac{2a_\mathrm{L}}{(\gamma - 1)} \left[\left(\frac{p}{p_\mathrm{L}} \right)^{\frac{\gamma - 1}{2\gamma}} - 1 \right] & \text{if } p \le p_\mathrm{L} \text{ (rarefaction)} \ , \end{cases} \tag{3.2}$$

the function f_R is given by

$$f_\mathrm{R}(p, \mathbf{W}_\mathrm{R}) = \begin{cases} (p - p_\mathrm{R}) \left[\frac{A_\mathrm{R}}{p + B_\mathrm{R}} \right]^{\frac{1}{2}} & \text{if } p > p_\mathrm{R} \text{ (shock)} \\ \frac{2a_\mathrm{R}}{(\gamma - 1)} \left[\left(\frac{p}{p_\mathrm{R}} \right)^{\frac{\gamma - 1}{2\gamma}} - 1 \right] & \text{if } p \le p_\mathrm{R} \text{ (rarefaction)} \end{cases} \tag{3.3}$$

and the data-dependent constants $A_\mathrm{L}, B_\mathrm{L}, A_\mathrm{R}, B_\mathrm{R}$ are given by

$$\left.\begin{aligned} A_{\mathrm{L}} &= \frac{2}{(\gamma+1)\rho_{\mathrm{L}}}, B_{\mathrm{L}} = \frac{(\gamma-1)}{(\gamma+1)} p_{\mathrm{L}} \\ A_{\mathrm{R}} &= \frac{2}{(\gamma+1)\rho_{\mathrm{R}}}, B_{\mathrm{R}} = \frac{(\gamma-1)}{(\gamma+1)} p_{\mathrm{R}} \end{aligned}\right\} \tag{3.4}$$

The solution for the particle velocity u_* in the Star Region is

$$u_* = \frac{1}{2}(u_{\mathrm{L}} + u_{\mathrm{R}}) + \frac{1}{2}[f_{\mathrm{R}}(p_*) - f_{\mathrm{L}}(p_*)] \tag{3.5}$$

Remark 3.2. Before proceeding to prove the above statements we make some useful remarks. Once (3.1) is solved for p_* the solution for u_* follows as in (3.9) and the remaining unknowns are found by using standard gas dynamics relations. The function f_{L} governs relations across the left non-linear wave and serves to connect the unknown particle speed u_* to the known state $\mathbf{W}_{\mathrm{L}}$ on the left side, see Fig. 3.3; the relations depend on the type of wave (shock or rarefaction). The arguments of f_{L} are the pressure p and the data state $\mathbf{W}_{\mathrm{L}}$. Similarly, the function f_{R} governs relations across the right wave and connects the unknown u_* to the right data state $\mathbf{W}_{\mathrm{R}}$; its arguments are p and $\mathbf{W}_{\mathbf{R}}$. For convenience we shall often omit the data arguments of the functions f, f_L and f_R. The sought pressure p_* in the Star Region is the root of the algebraic equation (4.1), $f(p) = 0$. A detailed analysis of the pressure function $f(p)$ reveals a particularly simple behaviour and that for physically relevant data there exists a unique solution to the equation $f(p) = 0$.

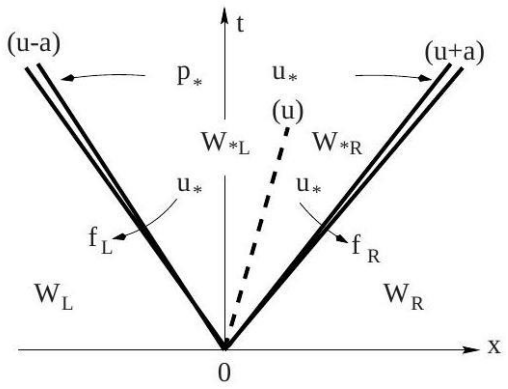

Fig. 3.3. Strategy for solving the Riemann problem via a pressure function. The particle velocity is connected to data on the left and right via functions f_{L} and f_{R}

3.1.1 Function f_{L} for a Left Shock

We assume the left wave is a shock moving with speed S_{L} as shown in Fig. 3.4a; pre-shock values are $\rho_{\mathrm{L}}, u_{\mathrm{L}}$ and p_{L} and post-shock values are $\rho_{*\,\mathrm{L}}, u_*$ and p_*.

As done in Sect. 3.1.3 of Chap. 3, we transform the equations to a frame of reference moving with the shock, as depicted in Fig. 3.4b. In the new frame the shock speed is zero and the relative velocities are

$$\hat{u}_{\mathrm{L}} = u_{\mathrm{L}} - S_{\mathrm{L}}, \hat{u}_{*} = u_{*} - S_{\mathrm{L}} \tag{3.6}$$

The Rankine-Hugoniot Conditions, see Sect. 3.1.3 of Chap. 3, give

$$\rho_{\mathrm{L}}\hat{u}_{\mathrm{L}} = \rho_{*\,\mathrm{L}}\hat{u}_{*} \tag{3.7}$$

$$\rho_{\mathrm{L}}\hat{u}_{\mathrm{L}}^{2} + p_{\mathrm{L}} = \rho_{*\,\mathrm{L}}\hat{u}_{*}^{2} + p_{*} \tag{3.8}$$

$$\hat{u}_{\mathrm{L}}\left(\hat{E}_{\mathrm{L}} + p_{\mathrm{L}}\right) = \hat{u}_{*}\left(\hat{E}_{*\,\mathrm{L}} + p_{*}\right) \tag{3.9}$$

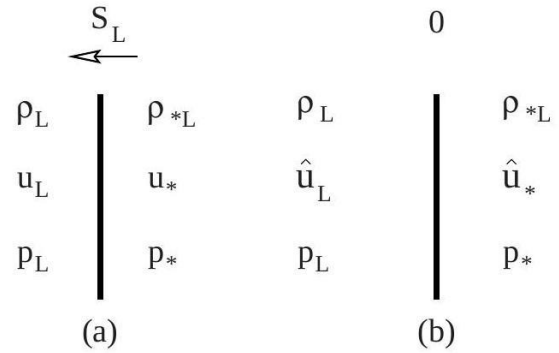

Fig. 3.4. Left wave is a shock wave of speed S_L : (a) stationary frame, shock speed is S_L (b) frame of reference moving with speed S_L, shock speed is zero

We introduce the mass flux Q_{L}, which in view of (3.7) may be written as

$$Q_{\mathrm{L}} \equiv \rho_{\mathrm{L}}\hat{u}_{\mathrm{L}} = \rho_{*\,\mathrm{L}}\hat{u}_{*} \tag{3.10}$$

From equation (3.8)

$$(\rho_{\mathrm{L}}\hat{u}_{\mathrm{L}})\hat{u}_{\mathrm{L}} + p_{\mathrm{L}} = (\rho_{*\,\mathrm{L}}\hat{u}_{*})\hat{u}_{*} + p_{*}$$

Use of (3.10) and solving for Q_{L} gives

$$Q_{\mathrm{L}} = -\frac{p_{*} - p_{\mathrm{L}}}{\hat{u}_{*} - \hat{u}_{\mathrm{L}}} \tag{3.11}$$

But from equation (3.6) $\hat{u}_{\mathrm{L}} - \hat{u}_{*} = u_{\mathrm{L}} - u_{*}$ and so Q_{L} becomes

$$Q_{\mathrm{L}} = -\frac{p_{*} - p_{\mathrm{L}}}{u_{*} - u_{\mathrm{L}}} \tag{3.12}$$

from which we obtain

$$u_{*} = u_{\mathrm{L}} - \frac{(p_{*} - p_{\mathrm{L}})}{Q_{\mathrm{L}}} \tag{3.13}$$

We are now close to having related u_{*} to data on the left hand side. We seek to express the right hand side of (3.13) purely in terms of p_{*} and $\mathbf{W}_{\mathrm{L}}$, which means that we need to express Q_{L} as a function of p_{*} and the data on the left hand side. We substitute the relations

$$\hat{u}_{\mathrm{L}} = \frac{Q_{\mathrm{L}}}{\rho_{\mathrm{L}}},\ \hat{u}_{*} = \frac{Q_{\mathrm{L}}}{\rho_{*\,\mathrm{L}}}$$

obtained from (3.10) into equation (3.11) to produce

$$Q_{\mathrm{L}}^2 = -\frac{p_* - p_{\mathrm{L}}}{\dfrac{1}{\rho_{*\,\mathrm{L}}} - \dfrac{1}{\rho_{\mathrm{L}}}} \tag{3.14}$$

As seen in Sect. 3.1.3 of Chap. 3, the density $\rho_{*\,\mathrm{L}}$ is related to the pressure p_* behind the left shock via

$$\rho_{*\,\mathrm{L}} = \rho_{\mathrm{L}} \left[\frac{\left(\frac{\gamma-1}{\gamma+1}\right) + \left(\frac{p_*}{p_{\mathrm{L}}}\right)}{\left(\frac{\gamma-1}{\gamma+1}\right)\left(\frac{p_*}{p_{\mathrm{L}}}\right) + 1} \right] \tag{3.15}$$

Substitution of $\rho_{*\,\mathrm{L}}$ into (3.14) yields

$$Q_{\mathrm{L}} = \left[\frac{p_* + B_{\mathrm{L}}}{A_{\mathrm{L}}} \right]^{\frac{1}{2}} \tag{3.16}$$

which in turn reduces (3.13) to

$$u_* = u_{\mathrm{L}} - f_{\mathrm{L}}(p_*, \mathbf{W}_{\mathrm{L}}), \tag{3.17}$$

with

$$f_{\mathrm{L}}(p_*, \mathbf{W}_{\mathrm{L}}) = (p_* - p_{\mathrm{L}}) \left[\frac{A_{\mathrm{L}}}{p_* + B_{\mathrm{L}}} \right]^{\frac{1}{2}}$$

and

$$A_{\mathrm{L}} = \frac{2}{(\gamma+1)\rho_{\mathrm{L}}},\ B_{\mathrm{L}} = \frac{(\gamma-1)}{(\gamma+1)} p_{\mathrm{L}}$$

Thus, the sought expression for f_{L} for the case in which the left wave is a shock wave has been obtained.

3.1.2 Function f_{L} for Left Rarefaction

Now we derive an expression for f_{L} for the case in which the left wave is a rarefaction wave, as shown in Fig. 3.5. The unknown state $\mathbf{W}_{*\,\mathrm{L}}$ is now connected to the left data state $\mathbf{W}_{\mathrm{L}}$ using the isentropic relation and the Generalised Riemann Invariants for the left wave. As seen in Sect. 3.1.2 of

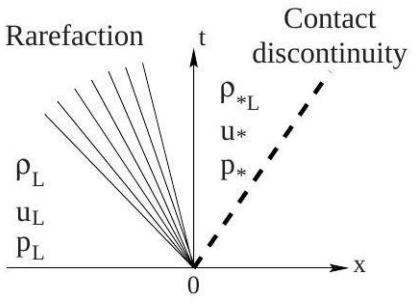

Fig. 3.5. Left wave is a rarefaction wave that connects the data state $\mathbf{W}_L$ with the unknown state $\mathbf{W}_{*L}$ in the star region to the left of the contact discontinuity

Chap. 3, the isentropic law

$$p = C\rho^{\gamma} \tag{3.18}$$

where C is a constant, may be used across rarefactions. C is evaluated at the initial left data state by applying the isentropic law, namely

$$p_{\mathrm{L}} = C\rho_{\mathrm{L}}^{\gamma}$$

and so the constant C is

$$C = p_{\mathrm{L}}/\rho_{\mathrm{L}}^{\gamma}$$

from which we write

$$\rho_{*\,\mathrm{L}} = \rho_{\mathrm{L}}\left(\frac{p_*}{p_{\mathrm{L}}}\right)^{\frac{1}{\gamma}} \tag{3.19}$$

In Sect. 3.1.3 of Chap. 3 we showed that across a left rarefaction the Generalised Riemann Invariant $I_{\mathrm{L}}(u, a)$ is constant. By evaluating the constant on the left data state we write

$$u_{\mathrm{L}} + \frac{2a_{\mathrm{L}}}{\gamma - 1} = u_* + \frac{2a_{*\,\mathrm{L}}}{\gamma - 1} \tag{3.20}$$

where a_{L} and $a_{*\,\mathrm{L}}$ denote the sound speed on the left and right states bounding the left rarefaction wave. See Fig. 3.5.

Substitution of $\rho_{*\,\mathrm{L}}$ from (3.19) into the definition of $a_{*\,\mathrm{L}}$ gives

$$a_{*\,\mathrm{L}} = a_{\mathrm{L}}\left(\frac{p_*}{p_{\mathrm{L}}}\right)^{\frac{\gamma-1}{2\gamma}} \tag{3.21}$$

and equation (3.20) leads to

$$u_* = u_{\mathrm{L}} - f_{\mathrm{L}}(p_*, \mathbf{W}_{\mathrm{L}}) \tag{3.22}$$

with

$$f_{\mathrm{L}}(p_*, \mathbf{W}_{\mathrm{L}}) = \frac{2a_{\mathrm{L}}}{(\gamma-1)}\left[\left(\frac{p_*}{p_{\mathrm{L}}}\right)^{\frac{\gamma-1}{2\gamma}} - 1\right]$$

This is the required expression for the function f_{L} for the case in which the left wave is a rarefaction wave.

3.1.3 Function f_{R} for a Right Shock

Here we find the expression for the function f_{R} for the case in which the right wave is a shock wave travelling with speed S_{R}. The situation is entirely analogous to the case of a left shock wave. Pre-shock values are $\rho_{\mathrm{R}}, u_{\mathrm{R}}$ and p_{R} and post-shock values are $\rho_{*\mathrm{R}}, u_*$ and p_*. In the transformed frame of reference moving with the shock, the shock speed is zero and the relative velocities are

$$\hat{u}_{\mathrm{R}} = u_{\mathrm{R}} - S_{\mathrm{R}}, \hat{u}_* = u_* - S_{\mathrm{R}} \tag{3.23}$$

Application of the Rankine-Hugoniot conditions gives

$$\left.\begin{aligned} &\rho_{*\mathrm{R}}\hat{u}_* = \rho_{\mathrm{R}}\hat{u}_{\mathrm{R}} \\ &\rho_{*\mathrm{R}}\hat{u}_*^2 + p_* = \rho_{\mathrm{R}}\hat{u}_{\mathrm{R}}^2 + p_{\mathrm{R}} \\ &\hat{u}_*\left(\hat{E}_{*\mathrm{R}} + p_*\right) = \hat{u}_{\mathrm{R}}\left(\hat{E}_{\mathrm{R}} + p_{\mathrm{R}}\right) \end{aligned}\right\} \tag{3.24}$$

Now the mass flux is defined as

$$Q_{\mathrm{R}} \equiv -\rho_{*\mathrm{R}}\hat{u}_* = -\rho_{\mathrm{R}}\hat{u}_{\mathrm{R}} \tag{3.25}$$

By performing algebraic manipulations similar to those for a left shock we derive the following expression for the mass flux

$$Q_{\mathrm{R}} = \left[\frac{p_* + B_{\mathrm{R}}}{A_{\mathrm{R}}}\right]^{\frac{1}{2}} \tag{3.26}$$

Hence the particle velocity in the Star Region satisfies

$$u_* = u_{\mathrm{R}} + f_{\mathrm{R}}(p_*, \mathbf{W}_{\mathrm{R}}) \tag{3.27}$$

with

$$f_{\mathrm{R}}(p_*, \mathbf{W}_{\mathrm{R}}) = (p_* - p_{\mathrm{R}})\left[\frac{A_{\mathrm{R}}}{p_* + B_{\mathrm{R}}}\right]^{\frac{1}{2}}$$
$$A_{\mathrm{R}} = \frac{2}{(\gamma+1)\rho_{\mathrm{R}}},\ B_{\mathrm{R}} = \frac{(\gamma-1)}{(\gamma+1)}p_{\mathrm{R}}$$

This is the sought expression for f_{R} for the case in which the right wave is a shock wave.

3.1.4 Function f_R for a Right Rarefaction

The derivation of the function f_{R} for the case in which the right wave is a rarefaction wave is carried out in an entirely analogous manner to the case of a left rarefaction. The isentropic law gives

$$\rho_{*\mathrm{R}} = \rho_{\mathrm{R}} \left(\frac{p_*}{p_{\mathrm{R}}}\right)^{\frac{1}{\gamma}} \tag{3.28}$$

and the Generalised Riemann Invariant $I_{\mathrm{R}}(u, a)$ for a right rarefaction gives

$$u_* - \frac{2a_{*\mathrm{R}}}{\gamma - 1} = u_{\mathrm{R}} - \frac{2a_{\mathrm{R}}}{\gamma - 1} \tag{3.27}$$

Using (3.28) into the definition of sound speed $a_{*\mathrm{R}}$ gives

$$a_{*\mathrm{R}} = a_{\mathrm{R}} \left(\frac{p_*}{p_{\mathrm{R}}}\right)^{\frac{\gamma-1}{2\gamma}} \tag{3.28}$$

which if substituted into (3.27) leads to

$$u_* = u_{\mathrm{R}} + f_{\mathrm{R}}(p_*, \mathbf{W}_{\mathrm{R}}) \tag{3.29}$$

with

$$f_{\mathrm{R}}(p_*, \mathbf{W}_{\mathrm{R}}) = \frac{2a_{\mathrm{R}}}{\gamma - 1}\left[\left(\frac{p_*}{p_{\mathrm{R}}}\right)^{\frac{\gamma-1}{2\gamma}} - 1\right]$$

The functions f_{L} and f_{R} have now been determined for all four possible wave patterns of Fig. 3.2. Now by eliminating u_* from equations (3.17) or (3.22) and (3.27) or (3.29) we obtain a single equation

$$f(p_*, \mathbf{W}_{\mathrm{L}}, \mathbf{W}_{\mathrm{R}}) \equiv f_{\mathrm{L}}(p_*, \mathbf{W}_{\mathrm{L}}) + f_{\mathrm{R}}(p_*, \mathbf{W}_{\mathrm{R}}) + \Delta u = 0 \tag{3.30}$$

which is the required equation (3.5) for the pressure. This proves the first part of the proposition. Assuming this single non-linear algebraic equation is solved (numerically) for p_* then the solution for the particle velocity u_* can be found from equation (3.17) if the left wave is a shock ($p_* > p_{\mathrm{L}}$) or from equation (3.22) if the left wave is a rarefaction ($p_* \leq p_{\mathrm{L}}$) or from equation (3.27) if the right wave is a shock ($p_* > p_{\mathrm{R}}$) or from equation (3.29) if the right wave is a rarefaction wave ($p_* \leq p_{\mathrm{R}}$). It can also be found from a mean value as

$$u_* = \frac{1}{2}(u_{\mathrm{L}} + u_{\mathrm{R}}) + \frac{1}{2}[f_{\mathrm{R}}(p_*) - f_{\mathrm{L}}(p_*)]$$

which is equation (3.9), and the proposition has thus been proved.

3.2 Numerical Tests

Five Riemann problems are selected to test the performance of the Riemann solver and the influence of the initial guess for pressure. The tests are also used to illustrate some typical wave patterns resulting from the solution of the Riemann problem. Table 3.1 shows the data for all five tests in terms of primitive variables. In all cases the ratio of specific heats is $\gamma = 1.4$.

Test 1 is the so called Sod test problem; this is a very mild test and its solution consists of a left rarefaction, a contact and a right shock. Fig. 3.6 shows solution profiles for density, velocity, pressure and specific internal energy across the complete wave structure, at time $t = 0.25$ units. Test 2 , called the 123 problem, has solution consisting of two strong rarefactions and a trivial stationary contact discontinuity; the pressure p_* is very small (close to vacuum) and this can lead to difficulties in the iteration scheme to find p_* numerically. Fig. 3.7 shows solution profiles. Test 2 is also useful in assessing the performance of numerical methods for low density flows. Test 3 is a very severe test problem, the solution of which contains a left rarefaction, a contact and a right shock; this test is actually the left half of the blast wave problem of Woodward and Colella, Fig. 3.8 shows solution profiles. Test 4 is the right half of the Woodward and Colella problem; its solution contains a left shock, a contact discontinuity and a right rarefaction, as shown in Fig. 3.9. Test 5 is made up of the right and left shocks emerging from the solution to tests 3 and 4 respectively; its solution represents the collision of these two strong shocks and consists of a left facing shock (travelling very slowly to the right), a right travelling contact discontinuity and a right travelling shock wave. Fig. 3.10 shows solution profiles for Test 5.

Test	ρ_L	u_L	p_L	ρ_R	u_R	p_R
1	1.0	0.0	1.0	0.125	0.0	0.1
2	1.0	-2.0	0.4	1.0	2.0	0.4
3	1.0	0.0	1000.0	1.0	0.0	0.01
4	1.0	0.0	0.01	1.0	0.0	100.0
5	5.99924	19.5975	460.894	5.99242	-6.19633	46.0950

Table 3.1. Data for five Riemann problem tests

Table 3.2 shows the computed values for pressure in the Star Region by solving the pressure equation $f(p) = 0$ (equation 3.5) by a Newton-Raphson method. This task is carried out by the subroutine STARPU, which is contained in the FORTRAN 77 program given in Sect. 3.9 of this chapter.

Test	p_*	p_{TR}	p_{PV}	p_{TS}	$\frac{1}{2}(p_{\mathrm{L}} + p_{\mathrm{R}})$
1	0.30313	0.30677(3)	0.55000(5)	0.31527(3)	0.55(5)
2	0.00189	exact (1)	TOL (8)	TOL (8)	0.4(9)
3	460.894	912.449(5)	500.005(4)	464.24(3)	500.005(4)
4	46.0950	82.9831(5)	50.005(4)	46.4162(3)	50.005(4)
5	1691.64	2322.65(4)	781.353(5)	1241.21(4)	253.494(6)

Table 3.2 Guess values p_0 for iteration scheme. Next to each guess is the required number of iterations for convergence (in parentheses).

$p_{\mathrm{PV}}, p_{\mathrm{TR}}$ and p_{TS}. In a typical application of the exact Riemann solver to a numerical method, the overwhelming majority of Riemann problems will consist of nearby states which can be accurately approximated by the simple value p_{PV}.

Having found p_*, the solution u_* for the particle velocity follows from (3.9) and the density values $\rho_{*\,\mathrm{L}}, \rho_{*\mathrm{R}}$ follow from appropriate wave relations, as detailed in the next section. Table 3.3 shows exact solutions for pressure p_*, speed u_*, densities $\rho_{*\,\mathrm{L}}$ and $\rho_{*\mathrm{R}}$ for tests 1 to 5 . These quantities may prove of some use for initial testing of programs.

Test	p_*	u_*	$\rho_{*\,\mathrm{L}}$	$\rho_{*\mathrm{R}}$
1	0.30313	0.92745	0.42632	0.26557
2	0.00189	0.00000	0.02185	0.02185
3	460.894	19.5975	0.57506	5.99924
4	46.0950	-6.19633	5.99242	0.57511
5	1691.64	8.68975	14.2823	31.0426

Table 3.3. Exact solution for pressure, speed and densities for tests 1 to 5.

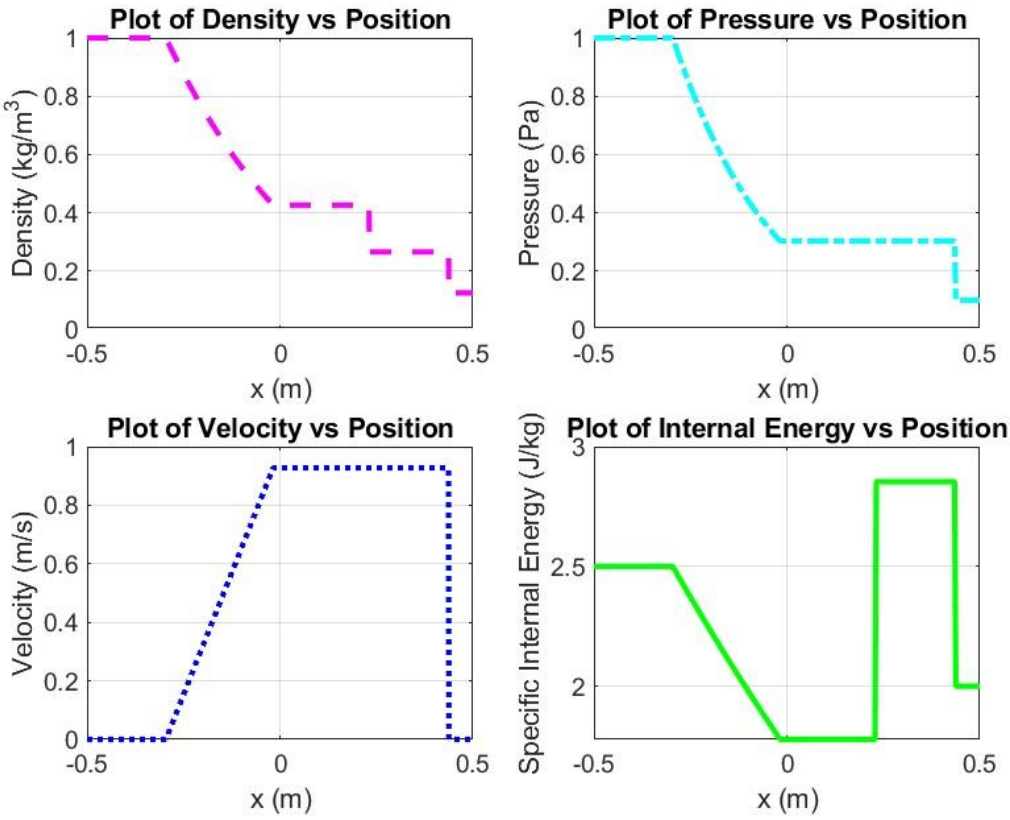

Fig 3.6 Plot produced using MATLAB for Test-1

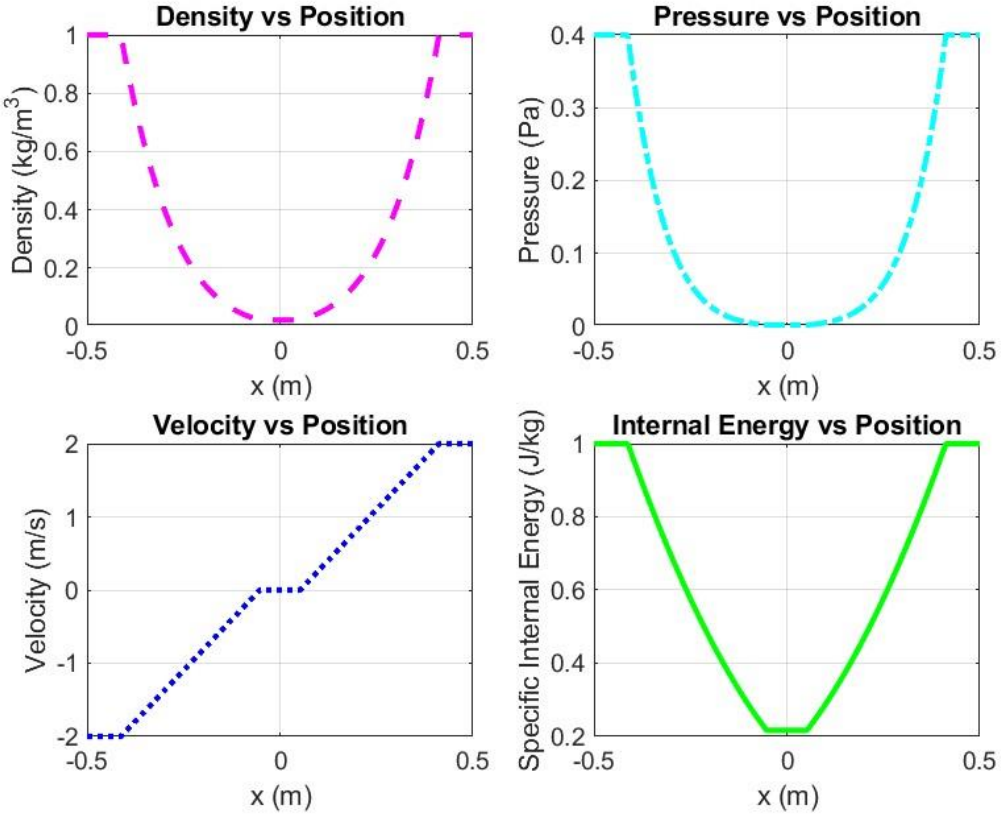

Fig 3.7 Plot produced using MATLAB for Test-2

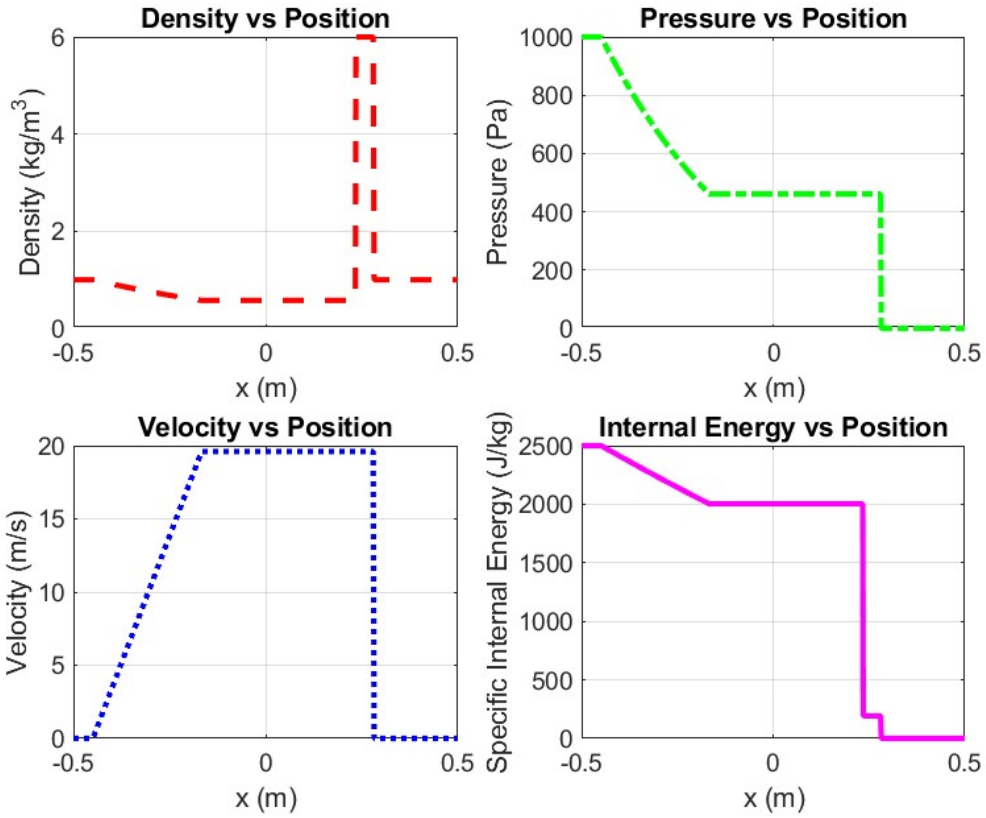

Fig 3.8 Plot produced using MATLAB for Test-3

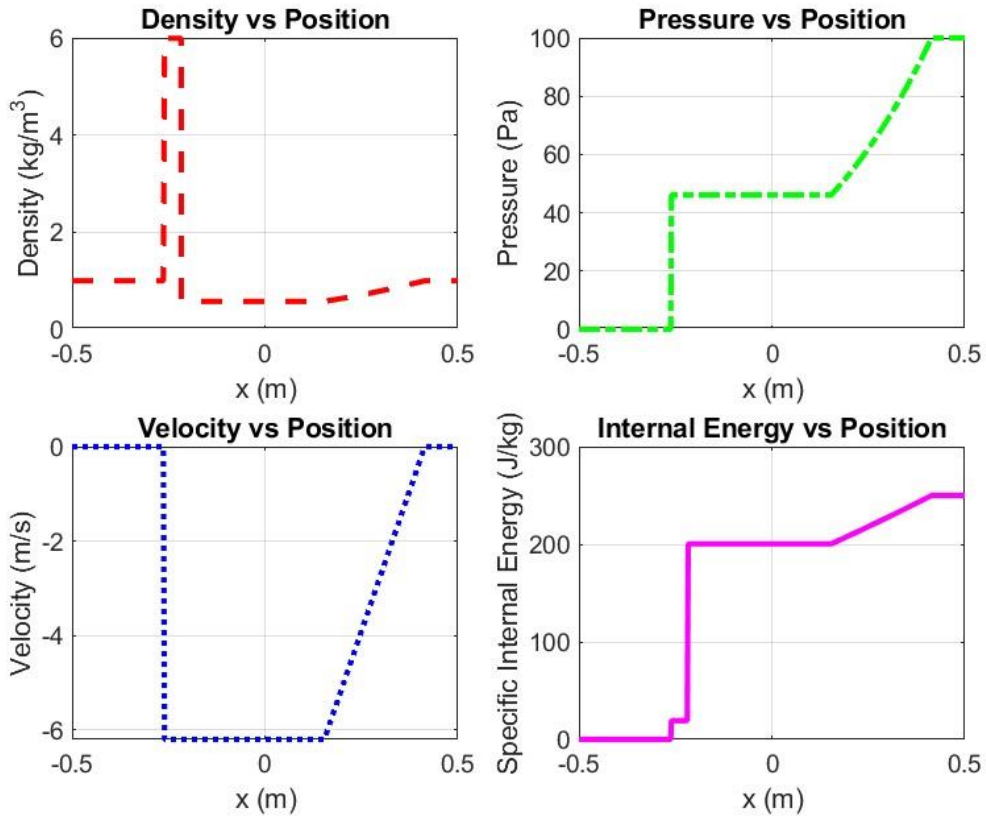

Fig 3.9 Plot produced using MATLAB for Test-4

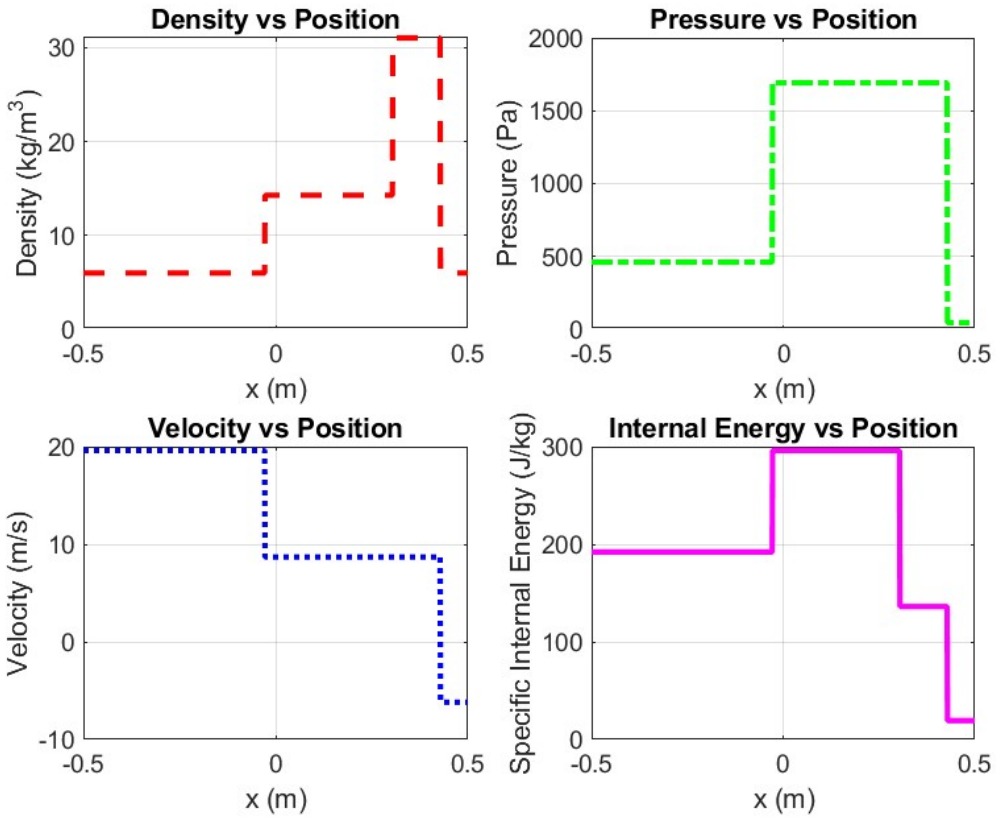

Fig 3.10 Plot produced using MATLAB for Test-5

4: Numerical Solution Using Iterative Schemes

4.1 Some Well-Known Schemes

Another first-order scheme is that of Lax and Friedrichs. The scheme is sometimes also called the Lax Method, or the scheme of Keller and Lax. This does not require the differencing to be performed according to upwind directions and can be seen as a way of stabilizing the unstable scheme obtained from forward in time and central in space approximations to the partial derivatives. The **Lax-Friedrichs** scheme results if u_i^n in the time derivative is replaced by

$$\frac{1}{2}(u_{i-1}^n + u_{i+1}^n)$$

a mean value of the two neighbors at time level n. Then the modified scheme becomes

$$u_i^{n+1} = \frac{1}{2}(u_{i-1}^n + u_{i+1}^n) - \frac{1}{2}c(u_{i+1}^n - u_{i-1}^n)$$

or

$$u_i^{n+1} = \frac{1}{2}(1+c)u_{i-1}^n + \frac{1}{2}(1-c)u_{i+1}^n \tag{4.1}$$

A von Neumann stability analysis reveals that scheme (4.1) is stable under the stability condition and a truncation error analysis says that the scheme is first-order accurate. The modified equation is like with numerical viscosity coefficient given by

$$\alpha_{\text{lf}} = \frac{\Delta x a}{2c}(1-c^2) \tag{4.2}$$

By comparing α_{lf} with α_{cir} we see that the **Lax-Friedrichs** scheme is considerably more diffusive than the CIR scheme; in fact for $0 \leq c \leq 1$ we have

$$2 \leq \alpha_{\text{lf}}/\alpha_{\text{cir}} = \frac{1+c}{c} < \infty$$

When written in the form the coefficients of the **Lax-Friedrichs** scheme are found to be

$$b_{-1} = \frac{1}{2}(1+c),\ b_0 = 0,\ b_1 = \frac{1}{2}(1-c)$$

Under the stability condition all coefficients b_k in the **Lax-Friedrich** scheme (4.1) are positive or zero. Therefore the scheme is monotone.

A scheme of historic as well as practical importance is that of Lax and Wendroff [302]. For a comprehensive treatment of the family of **Lax-Wendroff**. The basic **Lax-Wendroff** scheme is second-order accurate in both space and time. There are several ways of deriving the scheme for the model equation in (4.7). A rather unconventional derivation is this: for the time derivative u_t insist on the first-order forward approximation (4.9); for the space derivative u_x take an average of the upwind (stable if $a > 0$) and downwind (unstable if $a > 0$) approximations (4.14) and (4.15) respectively, that is

$$u_x = \beta_1 \frac{u_i^n - u_{i-1}^n}{\Delta x} + \beta_2 \frac{u_{i+1}^n - u_i^n}{\Delta x} \tag{4.3}$$

If the coefficients β_1, β_2 are chosen as

$$\beta_1 = \frac{1}{2}(1 + c), \beta_2 = \frac{1}{2}(1 - c) \tag{4.4}$$

the resulting scheme is the **Lax-Wendroff** method

$$u_i^{n+1} = \frac{1}{2}c(1 + c)u_{i-1}^n + (1 - c^2)u_i^n - \frac{1}{2}c(1 - c)u_{i+1}^n \tag{4.5}$$

This scheme is second-order in space and time although all finite difference approximations used to generate it are first-order accurate. Moreover, one of the terms in the spatial derivative originates from an unconditionally unstable scheme and yet the **Lax-Wendroff** scheme is stable with stability condition. This scheme is a good example to show that the order of accuracy of the scheme cannot in general be inferred from the order of accuracy of the finite difference approximations to the partial derivatives involved.

When written in the form the **Lax-Wendroff** scheme (4.5) has coefficients

$$b_{-1} = \frac{(1 + c)c}{2},\ b_0 = 1 - c^2,\ b_1 = -\frac{(1 - c)c}{2}$$

Therefore this scheme is not monotone. Not all coefficients in (4.5) are positive or zero. The fact that a scheme is not monotone is associated with the phenomenon of spurious oscillations in the numerical solution in the vicinity of sharp gradients, such as at discontinuities

Another second-order accurate scheme for (4.7) is the upwind method of **Warming and Beam**. For positive speed a it reads

$$u_i^{n+1} = \frac{1}{2}c(c - 1)u_{i-2}^n + c(2 - c)u_{i-1}^n + \frac{1}{2}(c - 1)(c - 2)u_i^n \tag{4.6}$$

Note that the scheme is fully one-sided in the sense that all the mesh points involved, other than the centre of the stencil, are on the left hand side of the centre of the stencil.

There is an equivalent scheme for negative speed a. Clearly the Warming-Beam scheme is not monotone. The stability restriction for this scheme is

$$0 \leq |c| \leq 2 \tag{4.7}$$

The enlarged stability range means that one may advance in time with a larger time step Δt, which has a bearing on the efficiency of the scheme.

Second-order schemes such as the **Lax-Wendroff** and **Warming-Beam** and have modified equation of the form

$$q_t + aq_x = \beta q_{xxx} \tag{4.9}$$

which is a dispersive equation.

4.2 Godunov's Method

Consider the constant coefficient, linear hyperbolic system written in conservation-law form

$$\mathbf{U}_t + \mathbf{F}(\mathbf{U})_x = \mathbf{0},\ \mathbf{F}(\mathbf{U}) \equiv \mathbf{AU} \tag{4.10}$$

The Godunov first-order upwind method utilises the conservative formula (4.76) and requires the solution $\mathbf{U}_{i+\frac{1}{2}}(x/t)$ of the local Riemann problem $RP(\mathbf{U}_i^n, \mathbf{U}_{i+1}^n)$ for (4.10) to compute the intercell numerical flux

$$\mathbf{F}_{i+\frac{1}{2}} = \mathbf{F}\left(\mathbf{U}_{i+\frac{1}{2}}(0)\right) \tag{4.11}$$

Here $\mathbf{U}_{i+\frac{1}{2}}(0)$ is the value of the solution $\mathbf{U}_{i+\frac{1}{2}}(x/t)$ at $x/t = 0$ along the intercell boundary. As seen in Sect. 2.3.3 of Chap. 2, the solution

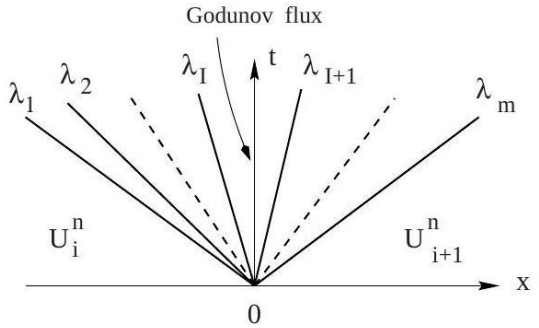

Fig. 4.1. Evaluation of the Godunov intercell flux for linear hyperbolic systems with constant coefficients

$\mathbf{U}_{i+\frac{1}{2}}(x/t)$ can be easily found by first expanding the initial data $\mathbf{U}_i^n, \mathbf{U}_{i+1}^n$ in terms of the right eigenvectors as

$$\mathbf{U}_i^n = \sum_{j=1}^{m} \alpha_j \mathbf{K}^{(j)},\ \mathbf{U}_{i+1}^n = \sum_{j=1}^{m} \beta_j \mathbf{K}^{(j)} \tag{4.12}$$

The general solution at any point (x, t) is given by

$$\mathbf{U}_{i+\frac{1}{2}}(x/t) = \sum_{j=1}^{I} \beta_j \mathbf{K}^{(j)} + \sum_{j=I+1}^{m} \alpha_j \mathbf{K}^{(j)} \tag{4.13}$$

where I is the largest integer with $1 \le I \le m$ such that $x/t \ge \lambda_I$. The Godunov flux (4.11) requires the solution at $x/t = 0$ in (4.13). See Fig. 4.1. For $x/t = 0I$ is such that $\lambda_I \le 0$ and $\lambda_{I+1} \ge 0$, then $\mathbf{U}_{i+\frac{1}{2}}(0)$ is obtained by manipulating (4.13), namely

$$\mathbf{U}_{i+\frac{1}{2}}(0) = \mathbf{U}_i^n + \sum_{j=1}^{I} \big(\beta_j - \alpha_j\big)\mathbf{K}^{(j)} \tag{4.14}$$

or

$$\mathbf{U}_{i+\frac{1}{2}}(0) = \mathbf{U}_{i+1}^n - \sum_{j=I+1}^{m} \big(\beta_j - \alpha_j\big)\mathbf{K}^{(j)} \tag{4.15}$$

Recall that the jump across wave j with eigenvalue λ_j and eigenvector $\mathbf{K}^{(j)}$ is given by $\big(\beta_j - \alpha_j\big)\mathbf{K}^{(j)}$. Note that the solution of the Riemann problem, at $x/t = 0$, as given by (4.14), can be interpreted as being the left data state $\mathbf{U}_i^n$ plus all wave jumps across waves of negative or zero speed. Similarly, the form (4.15) gives the solution as the right data state $\mathbf{U}_{i+1}^n$ minus the wave jumps across all waves of positive or zero speeds. By combining (4.14) and (4.15) we obtain

$$\mathbf{U}_{i+\frac{1}{2}}(0) = \frac{1}{2}(\mathbf{U}_i^n + \mathbf{U}_{i+1}^n) - \frac{1}{2}\sum_{j=1}^{m} \text{sign}\,\big(\lambda_j\big)\big(\beta_j - \alpha_j\big)\mathbf{K}^{(j)} \tag{4.16}$$

The Godunov intercell numerical flux (4.11) can now be obtained by evaluating $\mathbf{F}(\mathbf{U})$ at any of the expressions (4.14)-(4.16) for the solution of the Riemann problem. Use of (4.14) gives

$$\mathbf{F}_{i+\frac{1}{2}} = \mathbf{F}_i^n + \sum_{j=1}^{I} \mathbf{A}\big(\beta_j - \alpha_j\big)\mathbf{K}^{(j)} \tag{4.17}$$

and since $\mathbf{AKK}^{(j)} = \lambda_j \mathbf{K}^{(j)}$,

$$\mathbf{F}_{i+\frac{1}{2}} = \mathbf{F}_i^n + \sum_{j=1}^{I} (\beta_j - \alpha_j)\lambda_j \mathbf{K}^{(j)} \tag{4.18}$$

Similarly, (4.15) gives

$$\mathbf{F}_{i+\frac{1}{2}} = \mathbf{F}_{i+1}^n - \sum_{j=I+1}^{m} (\beta_j - \alpha_j)\lambda_j \mathbf{K}^{(j)} \tag{4.19}$$

or combining (4.18) and (4.19) we obtain

$$\mathbf{F}_{i+\frac{1}{2}} = \frac{1}{2}(\mathbf{F}_i^n + \mathbf{F}_{i+1}^n) - \frac{1}{2}\sum_{j=1}^{m} (\beta_j - \alpha_j)|\lambda_j|\mathbf{K}^{(j)} \tag{4.20}$$

Next we show that the Godunov flux can also be expressed in two more alternative forms.

Proposition 4.20. The Godunov flux (4.11) to solve (4.10) via (4.76) can be written as

$$\mathbf{F}_{i+\frac{1}{2}} = \frac{1}{2}(\mathbf{F}_i^n + \mathbf{F}_{i+1}^n) - \frac{1}{2}|\mathbf{A}|(\mathbf{U}_{i+1}^n - \mathbf{U}_i^n) \tag{4.21}$$

Proof. Starting from (4.20) and using the properties one writes

$$\begin{aligned}
\mathbf{F}_{i+\frac{1}{2}} &= \frac{1}{2}(\mathbf{F}_i^n + \mathbf{F}_{i+1}^n) - \frac{1}{2}\sum_{j=1}^{m} (\beta_j - \alpha_j)(\lambda_j^+ - \lambda_j^-)\mathbf{K}^{(j)} \\
&= \frac{1}{2}(\mathbf{F}_i^n + \mathbf{F}_{i+1}^n) - \frac{1}{2}\sum_{j=1}^{m} (\beta_j - \alpha_j)[\lambda_j^+ \mathbf{K}^{(j)} - \lambda_j^- \mathbf{K}^{(j)}] \\
&= \frac{1}{2}(\mathbf{F}_i^n + \mathbf{F}_{i+1}^n) - \frac{1}{2}\sum_{j=1}^{m} (\beta_j - \alpha_j)[\mathbf{A}^+ \mathbf{K}^{(j)} - \mathbf{A}^- \mathbf{K}^{(j)}] \\
&= \frac{1}{2}(\mathbf{F}_i^n + \mathbf{F}_{i+1}^n) - \frac{1}{2}\sum_{j=1}^{m} (\beta_j - \alpha_j)[\mathbf{A}^+ - \mathbf{A}^-]\mathbf{K}^{(j)} \\
&= \frac{1}{2}(\mathbf{F}_i^n + \mathbf{F}_{i+1}^n) - \frac{1}{2}|\mathbf{A}|\sum_{j=1}^{m} (\beta_j - \alpha_j)\mathbf{K}^{(j)}
\end{aligned}$$

Hence

$$\mathbf{F}_{i+\frac{1}{2}} = \frac{1}{2}(\mathbf{F}_i^n + \mathbf{F}_{i+1}^n) - \frac{1}{2}|\mathbf{A}|(\mathbf{U}_{i+1}^n - \mathbf{U}_i^n)$$

and the proposition is proved.

Proposition 4.1. The Godunov flux (4.11) for (4.10) can be written in flux-split form as

$$\mathbf{F}_{i+\frac{1}{2}} = \mathbf{A}^{+}\mathbf{U}_{i}^{n} + \mathbf{A}^{-}\mathbf{U}_{i+1}^{n} \tag{4.22}$$

Proof. The result follows directly from manipulating (4.21) and using appropriate definitions. Alternatively we have

$$\begin{aligned}
\mathbf{F}_{i+\frac{1}{2}} &= \mathbf{A}\mathbf{U}_{i+\frac{1}{2}}(0) \\
&= \sum_{j=1}^{I} \beta_j \mathbf{A}\mathbf{K}^{(j)} + \sum_{j=I+1}^{m} \alpha_j \mathbf{A}\mathbf{K}^{(j)} \\
&= \sum_{j=1}^{I} \beta_j \lambda_j \mathbf{K}^{(j)} + \sum_{j=I+1}^{m} \alpha_j \lambda_j \mathbf{K}^{(j)} \\
&= \sum_{j=1}^{m} \beta_j \lambda_j^{-} \mathbf{K}^{(j)} + \sum_{j=1}^{m} \alpha_j \lambda_j^{+} \mathbf{K}^{(j)} \\
&= \sum_{j=1}^{m} \beta_j \mathbf{A}^{-} \mathbf{K}^{(j)} + \sum_{j=1}^{m} \alpha_j \mathbf{A}^{+} \mathbf{K}^{(j)} \\
&= \mathbf{A}^{+} \sum_{j=1}^{m} \alpha_j \mathbf{K}^{(j)} + \mathbf{A}^{-} \sum_{j=1}^{m} \beta_i \mathbf{K}^{(j)} \\
&= \mathbf{A}^{+}\mathbf{U}_{i}^{n} + \mathbf{A}^{-}\mathbf{U}_{i+1}^{n}
\end{aligned}$$

and the proposition is proved.

Remark 4.1. The intercell flux has been split as

$$\mathbf{F}_{i+\frac{1}{2}} = \mathbf{F}_{i+\frac{1}{2}}^{+} + \mathbf{F}_{i+\frac{1}{2}}^{-} \tag{4.23}$$

where the positive $\mathbf{F}_{i+\frac{1}{2}}^{+}$and negative $\mathbf{F}_{i+\frac{1}{2}}^{-}$flux components are

$$\mathbf{F}_{i+\frac{1}{2}}^{+} = \mathbf{A}^{+}\mathbf{U}_{i}^{n},\ \mathbf{F}_{i+\frac{1}{2}}^{-} = \mathbf{A}^{-}\mathbf{U}_{i}^{n} \tag{4.24}$$

Note that, trivially, the respective Jacobian matrices have eigenvalues that are all positive (or zero) and all negative (or zero).

Exercise 4.1. Consider the linearised equations of Gas Dynamics

$$\mathbf{U}_t + \mathbf{A}\mathbf{U}_x = \mathbf{0}$$

with

$$\mathbf{U} = \begin{bmatrix} u_1 \\ u_2 \end{bmatrix} \equiv \begin{bmatrix} \rho \\ u \end{bmatrix}, \mathbf{A} = \begin{bmatrix} 0 & \rho_0 \\ a^2/\rho_0 & 0 \end{bmatrix}$$

- Find the matrices $\mathbf{\Lambda}^-, \mathbf{\Lambda}^+, \mathbf{A}^-, \mathbf{A}^+$.
- Write the scheme (4.93) in full, that is for the two components of the vector of unknowns.
- Compute the Godunov intercell flux directly by using the explicit solution of the Riemann problem in the Star Region

$$\left.\begin{aligned} \rho_* &= \frac{1}{2}(\rho_\mathrm{L} + \rho_\mathrm{R}) - \frac{1}{2}(u_\mathrm{R} - u_\mathrm{L})\rho_0/a \\ u_* &= \frac{1}{2}(u_\mathrm{L} + u_\mathrm{R}) - \frac{1}{2}(\rho_\mathrm{R} - \rho_\mathrm{L})a/\rho_0 \end{aligned}\right\}$$

Write a computer program to solve the linearised equations of Gas Dynamics using the method of Godunov.

4.3 Sample Numerical Results

To complete this chapter, we present some numerical results obtained by some of the most well known schemes as applied to two model PDEs.

4.3.1 Linear Advection

We apply four schemes to solve

$$u_t + f(u)_x = 0,\ f(u) = au,\ a = \text{ constant} \tag{4.25}$$

with two types of initial conditions.

Test 1 for linear advection (smooth data)

Here the initial condition is the smooth profile

$$u(x,0) = \alpha e^{-\beta x^2} \tag{4.26}$$

In the computations we take $a = 1.0, \alpha = 1.0, \beta = 8.0$ and a CFL coefficient $C_{\mathrm{cf}} = 0.8$; the initial profile $u(x,0)$ is evaluated in the interval $-1 \le x \le 1$. Computed results are shown in Figs. 4.9 to 4.11; these correspond respectively to the output times $t = 1.0$ unit (125 time steps), $t = 10.0$ units (1250 time steps), $t = 100.0$ units (12499 time steps). In each figure we compare the exact solution (shown by full lines) with the numerical solution

(symbols) for the Godunov method, the **Lax-Friedrichs** method, the **Lax-Wendroff** method and the Warming-Beam method.

The results of Fig. 4.9 are in many ways representative of the quality of each scheme. Collectively these results are also representative of most of the current successes and limitations of numerical methods for PDEs governing wave propagation. The first-order method of Godunov (CIR scheme) has modified equation of the form (4.24), where α_{cir} is a numerical viscosity coefficient. This is responsible for the clipping of the peak values. As seen earlier $\alpha_{\text{cir}} < \alpha_{\text{lf}}$, which explains the fact that the **Lax-Friedrichs** scheme gives even more diffused results. For the computational parameters used $\alpha_{\text{cir}} = 0.1\Delta x$ and $\alpha_{\text{lf}} = 0.225\Delta x$.

The results from the **Lax-Wendroff** method and the Warming-Beam method, both second-order accurate, are much more accurate than those of the first-order schemes. There are however, slight signs of error in the position of the wave. For the **Lax-Wendroff** scheme the computed wave lags behind the true wave (lagging phase error), while for the Warming-Beam method the computed wave is ahead of the true wave (leading phase error). The phase errors of second-order accurate schemes are explained by the dispersive term of the modified equation (4.9).

The limitations of the schemes are more clearly exposed if the solution is evolved for longer times. Fig. 4.10 shows results at the output time t =10.0 units (1250 time steps). Compare with Fig. 4.9. The numerical diffusion inherent in first-order methods has ruined the solution of the Godunov and **Lax-Friedrichs** schemes. Computed peak values are only of the order of 30 to 40% of the true peak values. The second-order methods are still giving more satisfactory results than their first-order counterparts, but now the numerical dispersion errors are clearly visible. Numerical diffusion is beginning to show its effects too.

Fig. 4.11 shows results at the output time $t = 100.0$ units (12499 time steps). Compare with Figs. 4.9. and 4.10. These results are truly disappointing and clearly expose the limitations of numerical methods for computing solutions to problems involving long time evolution of wave phenomena. In acoustics one may require the computation of (i) very weak signals (ii) over long distances. The combination of these two requirements rules out automatically a wide range of otherwise acceptable numerical methods for PDEs. See Tam and Webb [480]. The numerical diffusion of the first-order schemes has virtually flattened the wave, while the numerical dispersion of the second order methods has resulted in unacceptable position errors, in addition to clipping by numerical ffusion.

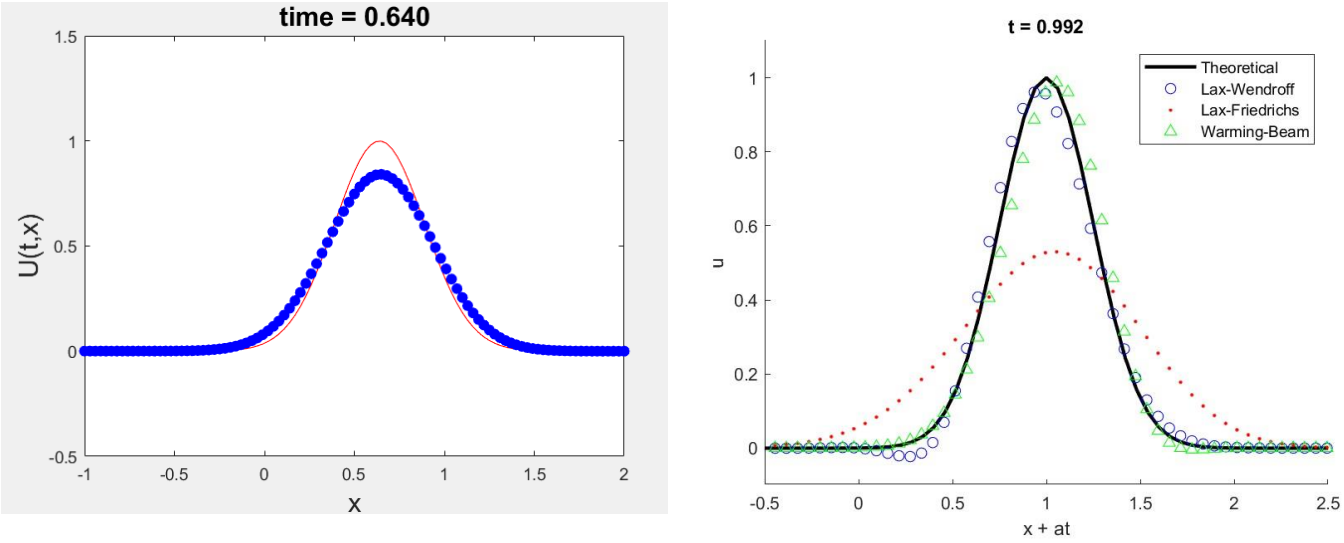

Fig 4.2 Plot produced using MATLAB for linear advection equation for smooth data at the given time

Test 2 for linear advection (discontinuous data)

Now the initial data for (4.25) consists of a square wave, namely

$$u(x,0) = \begin{cases} 0 & \text{if } x \leq 0.3 \\ 1 & \text{if } 0.3 \leq x \leq 0.7 \\ 0 & \text{if } x \geq 0.7 \end{cases} \tag{4.27}$$

The computed results for the three output times are shown in Figs. 4.12 to 4.14. As for Test 1 the effects of numerical diffusion in the first-order methods and the effects of dispersion in the second-order methods lead to visible errors in the numerical solution (symbols), as compared with the exact solution (full line). First-order methods smear discontinuities over many computing cells; as expected this error is more apparent in the **Lax-Friedrichs** scheme. Note also the pairing of neighbouring values in the **Lax-Friedrichs** scheme. Second-order methods reduce the smearing of discontinuities, but at the cost of overshoots and undershoots in the vicinity of the discontinuities. These spurious oscillations are highly undesirable features of second and higherorder methods. We shall return to this theme in Chaps. 13 and 14, where improved methods for dealing with discontinuities will be presented.

Fig. 4.13 shows results for Test 2 at time $t = 10.0$ units (1250 time steps). The errors observed in Fig. 4.12 are now exaggerated. Fig. 4.14 shows results at time $t = 100.0$ units (12499 time steps). Once again first-order methods have lost the solution while second-order methods exhibit unacceptable position errors, in addition to spurious oscillations

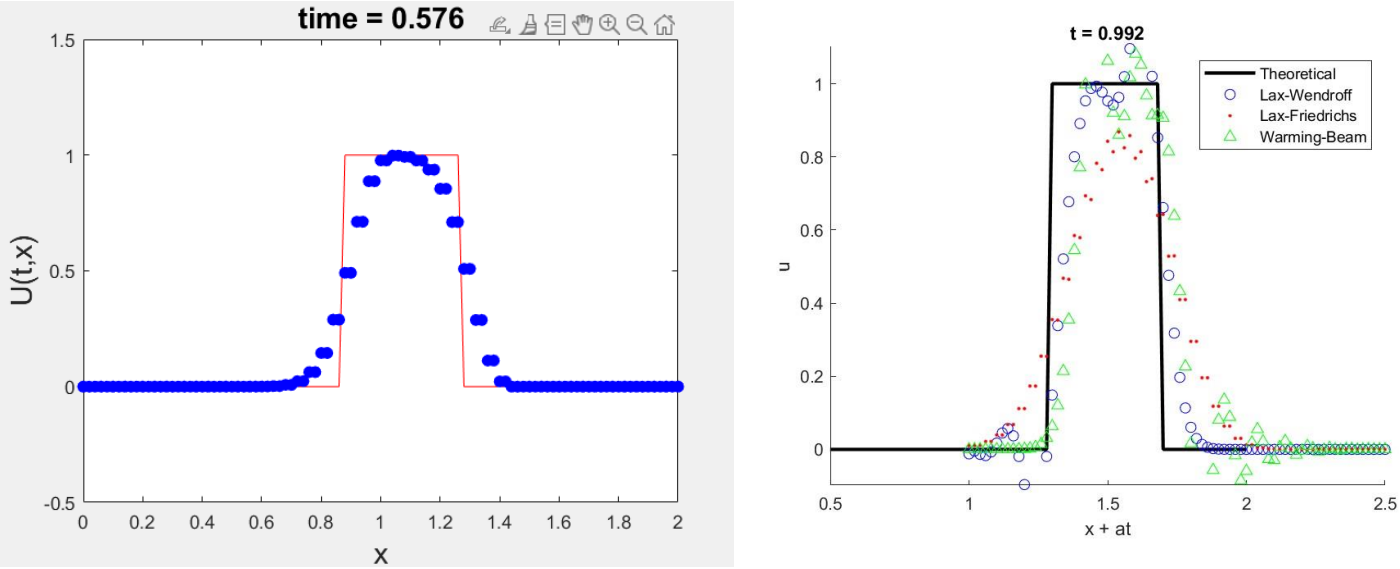

Fig 4.3 Plot produced using MATLAB for linear advection equation for discontinuous data at the given time

4.3.2 The Inviscid Burgers Equation

Our Test 3 consists of the inviscid Burgers equation

$$u_t + f(u)_x = 0,\ f(u) = \frac{1}{2}u^2 \tag{4.28}$$

in the domain $\left[0, \frac{3}{2}\right]$ with initial conditions

$$u(x,0) = \begin{cases} -\frac{1}{2} \text{ if } x \le \frac{1}{2} & (4.29) \\ 1 \text{ if } \frac{1}{2} \le x \le 1 & (4.29) \\ 0 \text{ if } x \ge 1 & (4.29) \end{cases}$$

We solve this problem numerically on a domain of length $L = 1.5$ discretised by $M = 75$ equally spaced cells of width $\Delta x = 0.02$; the CFL coefficient used is 0.8 . Fig. 4.15 shows computed results (symbol) along with the exact (line) solution, for the Godunov and **Lax-Friedrichs** schemes at time $t = 0.5$ units (32 time steps). Two new features are now present in solving non-linear PDEs. First the discontinuity on the right is a shock wave. This satisfies the entropy condition, see Sect. 2.4.2 of Chap. 2, and characteristics on either side of the discontinuity converge into the discontinuity. This compression mechanism helps the more accurate resolution of shock waves. Compare with Fig. 4.12.

The Godunov method resolves the shock much more sharply (3 cells) than the **Lax-Friedrichs** scheme (10 cells). The second new feature to note in this

non-linear example is the entropy glitch at $x = \frac{1}{2}$. The entropy glitch affects the Godunov method and not the **Lax-Friedrichs** method. A question of crucial importance is the construction of entropy satisfying schemes .

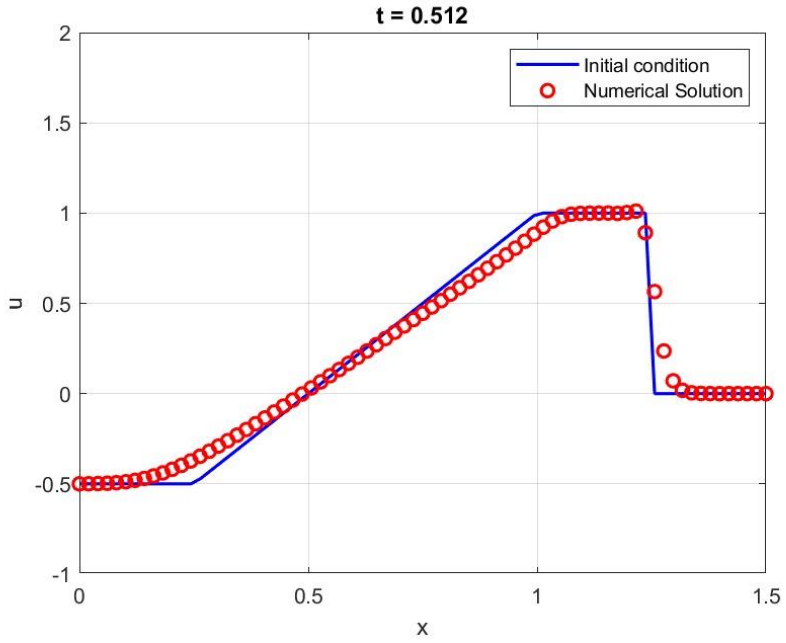

Fig 3.8 Plot produced using MATLAB for Inviscid Burgers Equation

4.4 Numerical Scheme Solutions for Riemann Problem

Performing the Godunov's scheme and Lax-Friedrichs scheme on Test-1 discussed earlier in Chapter 3 which is the so called Sod test problem; this is a very mild test and its solution consists of a left rarefaction, a contact and a right shock. Figure below shows solution profiles for density, velocity, pressure and specific internal energy across the complete wave structure, at time $t = 0.25$ units.

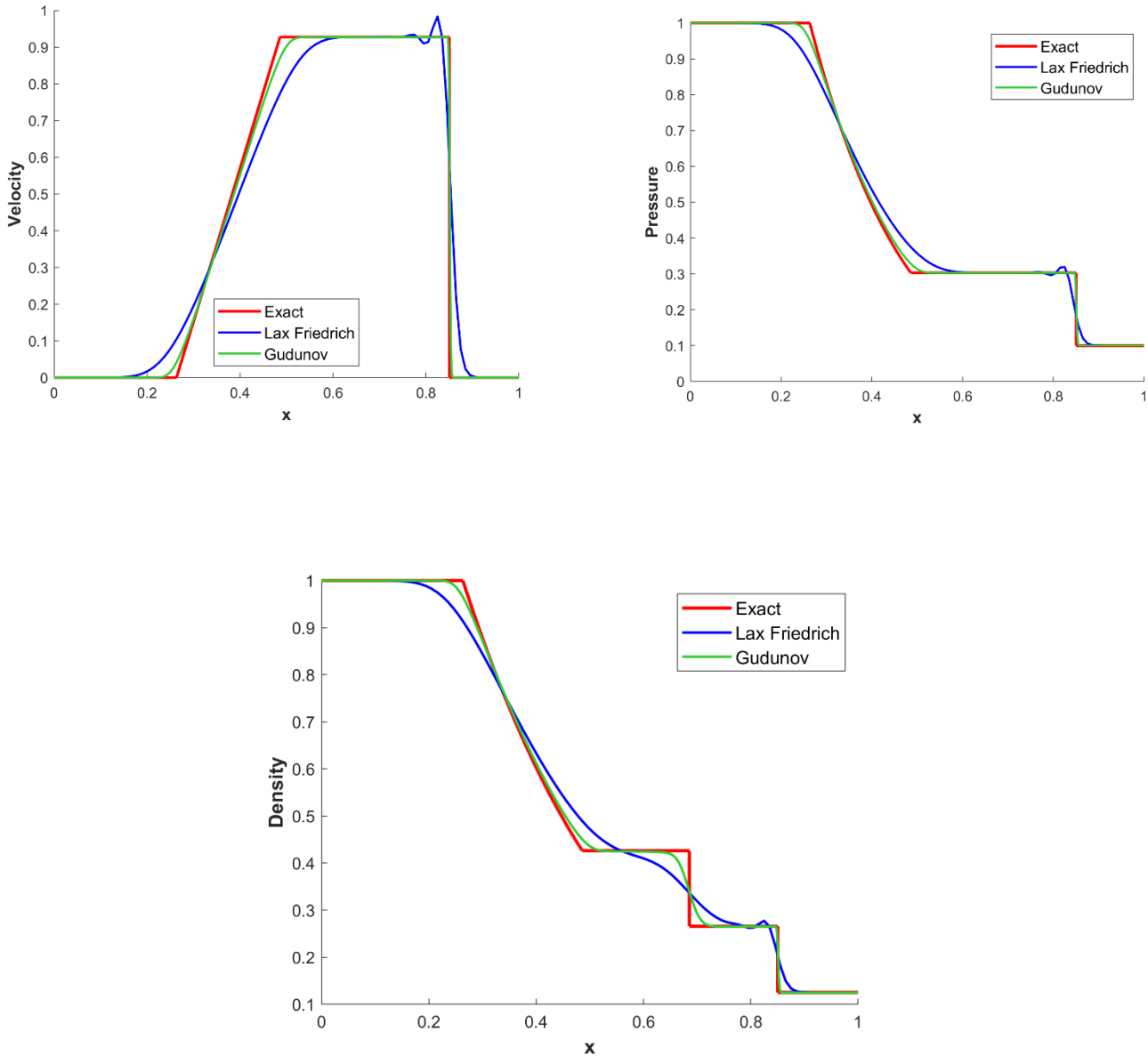

5: Conclusion

In conclusion, this project has been an enriching voyage into the realm of computational fluid dynamics, delving deeply into the intricacies of Riemann problems, shock waves, and rarefactions. Through meticulous study and hands-on implementation, I have garnered a profound understanding of various numerical methodologies, including Godunov's, Lax-Friedrichs, and Lax-Wendroff methods. By employing these techniques in MATLAB, I have gained practical insights into their behaviors, strengths, and limitations when applied to solving the linear advection equation.

Recognizing Riemann problems as fundamental to grasping wave behaviors, particularly shocks and rarefactions, underscores the criticality of employing accurate numerical approaches to capture these phenomena effectively. Moreover, juxtaposing exact solutions against numerical approximations has underscored the inherent trade-offs between computational efficiency and precision inherent in these methods.

In today's era, where computational simulations drive innovations across diverse sectors such as climate modeling and aerospace engineering, the significance of robust numerical methodologies in predicting complex wave behaviors cannot be overstated. The skills and knowledge acquired from this project resonate deeply with the current demand for precise and efficient simulations in our rapidly evolving technological landscape.

I express heartfelt gratitude to Professor Minhajul of the Department of Mathematics, BITS Pilani KK Birla Goa Campus, for his invaluable guidance, unwavering support, and the opportunity to work under his mentorship. His expertise and encouragement have been instrumental in shaping this project and fostering my growth in the field of Computational Fluid Dynamics.

6: References

[1] Eleuterio F. Toro. Riemann Solvers and Numerical Methods for Fluid Dynamics. Springer Berlin, Heidelberg, 3 edition, 2009.